CHAPTER 5 THREE-DIMENSIONAL ANALYSIS -- NUMERICAL MODEL B

5.1 INTRODUCTION

This chapter describes a three-dimensional analysis of a single full scale concrete pipe with surrounding soil. Emphasis of the analysis was placed on the interaction between the pipe and the surrounding soil. The results from numerical model A in Chapter 4 show that the computed stresses near the joint under the 'diagonal' load may be affected by the local constraints. This local effect was also examined in the analysis. In this chapter, a three-dimensional model, numerical model B, is described in Section 5.2. The analysis with elastic surrounding soil, the interaction between the pipe and the surrounding soil, and the analysis with plastic surrounding soil are discussed in Sections 5.3, 5.4 and 5.5 respectively. Section 5.6 gives the conclusion from the analysis with this model. Finally, a numerical back analysis of site measured data (Norris 1992) is described in Section 5.7.

5.2 NUMERICAL MODEL B

The numerical model B, a concrete pipe with surrounding soil, and its finite element mesh are shown in Figure 5.1 (again, since the geometry of the domain of the model B and the loads are symmetrical about the plane of $y = 0$, only half of the domain was used in analysis and shown in the figure). For simplicity, it was assumed in the analysis that there was no initial gap between the pipe and the surrounding soil and that there was no initial pressure on the pipe from the surrounding soil. The three-dimensional mesh is shown in Figure 5.1(a); the surface of r = constant unfolded on a plane is show n in Figure 5.1(b); the section of z = constant in Figure 5.1(c) and the section of $\theta = 0^0$ in Figure 5.1(d). The dimensions of the model are also shown in Figure 5.1(d). In the numerical analysis, the nodes on the outer surface of the soil mesh were all fixed in both x and y directions and on the symmetrical plane

$y = 0$ the nodes were all fixed in the y direction. The element type of 8-node hexahedron was used. The pipe was treated as linear elastic in the analysis and the material constants used by Norris (1992), the Young's modulus E_c = 40000MPa and the Poisson's ratio μ_c = 0.2, were adopted for convenience in order to compare the numerical results with his experimental data. The surrounding soil was taken as linear elastic except in the analysis described in Section 5.5 where the soil was modelled by an elastic-plastic Matsuoka model. (To examine the mesh sensitivity, the analyses were carried out with two, four and six layers of soil elements at first. The difference between the results with four layers of soil elements and those with six layers of soil element was small. So the analyses were carried out with four layers of soil elements for the parametric study described in this chapter.)

5.3 ANALYSIS WITH ELASTIC SOIL

In this section, the effect of the soil Young's modulus is investigated with the results from an elastic analysis. In the analysis, the surrounding soil was treated as linearly elastic with a Poisson's ratio μ_s = 0.2 and three different Young's moduli E_s = 144MPa, 14.4MPa and 1440MPa in three different analysis cases (SE1, SE2 and SE3). The Poisson's ratio and the first Young's modulus (E_s = 144MPa) were adopted from thesis of Norris (1992) to represent a typical soil (Das 1983, Bolton 1979), while the second and third Young's moduli were obtained from the first one by reducing and enlarging 10 times to model the arbitrary soft and stiff soil. Two different types of load, the 'edge' load and the 'diagonal' load , were also included in the analysis to examine the effect of the soil stiffness under different loading conditions. The two loads were used to simulate the two extreme loading conditions occurring in practice (Norris 1992) due to the misalignment of the pipe line during pipe jacking. The total load applied at each end of the pipe was the same P = 1000kN (on half of the pipe). The load distributions are shown in Figure 5.2(a) and 5.2(b) for the 'edge' and the 'diagonal' loading respectively (for clarity, the mesh of the surrounding soil is not included). The 'edge' load is distributed linearly in the x direction on both ends of the pipe as shown in

Figure 5.2(a). The distribution of the 'diagonal' load was the same as that of the 'edge' load on the upper pipe end, and the distribution on the bottom pipe end was obtained by rotating that of the 'edge' load by 180^0 in the θ direction.

If the applied load is uniformly distributed over the pipe end, the average pressure is q = 4.21MPa. The stresses shown in the contours in this chapter are all normalized with respect to this pressure for convenience of comparison. Furthermore, for a better view, the soil is excluded in all stress contours in this chapter since the study is on the behaviour of the concrete pipe.

5.3.1 EDGE LOADING

This section describes the effect of the soil stiffness under the 'edge' loading condition. The results of the normalized most tensile principal stresses in the pipe are shown in Figure 5.3. The results with the soil Young's modulus E_s = 144MPa (case SE1) is in Figure 5.3(a), the results with E_s = 14.4MPa (case SE2) in Figure 5.3(b) and the results with E_s = 1440MPa (case SE3) in Figure 5.3(c). From the figure, it is clear that in all three cases the stresses in the pipe are highly concentrated in two small domains adjacent to the loaded border at the pipe ends on the internal surface of the pipe; while the stresses in other regions are very small except that there are some tensile stresses at the middle length position of the pipe on the internal surface in the region of $\theta = 180^0$. The highest stress is in case SE2, while the peak value of the stresses in case SE3 is much lower than those in case SE1 and SE2. The results are symmetric to the plane of the middle length of pipe (z = 1250mm) since the load is also symmetric about this plane. The distribution of the principal direction is complex and difficult to be expressed in a three-dimensional contour. However, in all three cases the tensile stresses in the high stress domains are mainly in the hoop direction as shown in Figure 5.3(d).

The results of the normalized most compressive principal stresses in the pipe are shown in Figure 5.4. The results with E_s = 144MPa , 14.4MPa and 1440MPa are shown in Figures 5.4(a), 5.4(b) and 5.4(c) respectively. Again, the stress patterns in all three cases are similar except that in the case ES3 the magnitudes of the stresses at the middle length of the pipe in the region of $\theta > 110^0$ are much lower than those in the other two cases. The magnitudes of the stresses are very high in the region of $\theta = 180^0$ especially at the two loaded corners, and the stresses in the region of $\theta < 80^0$ are very small. In general, the magnitude of the stress on a plane z = constant reduces when θ decreases, and on a section of θ = constant, the magnitude of stress is high at the two ends of the pipe and reduces towards the middle of the pipe (z = 1250mm) in the region of $\theta > 80^0$ due to the friction between the pipe and the soil, especially in the case of stiff soil. (The friction between the pipe and surrounding soil is discussed in Section 5.4 with the interface elements. It should be pointed out that if a lubricant is used in pipe jacking, the friction between the pipe and the soil will reduce significantly under both the 'edge' and the 'diagonal' loading.) The change of magnitude across the pipe thickness is not significant. The maximum values of the stress magnitude are similar in all three cases.

5.3.2 DIAGONAL LOADING

Under the 'diagonal' loading condition, the load is transferred diagonally between opposite corners of the pipe as shown in Figure 5.2(b). Again, three cases (SD1, SD2 and SD3) with the same three different Young's moduli of the surrounding soil E_s = 144MPa, 14.4MPa and 1440MPa were adopted in the analysis.

The normalized most tensile principal stresses in the pipe under the 'diagonal' loading are shown in Figure 5.5(a), 5.5(b) and 5.5(c) for the case SD1, SD2 and SD3 respectively. From the figure, it is clear that in case SD1 and SD2 the stress patterns are similar. High tensile stresses are located near the loaded borders on the internal surface and at the two non-loaded

diagonal corners, and there is a low stress band in the region of $\theta = 90^0$ connecting the high stress domains near the loaded borders. In case SD3, the high stresses are mainly at the central area on the internal surface of the pipe in addition to the edge of the loaded area and the two non-loaded corners. It should be pointed out that the high tensile stresses on the external surface of the pipe at the two non-loaded corners are possibly due to the unrealistic high stresses acting on the external surface of the pipe at these areas from the surrounding elastic soil as shown in Figure 5.5(d). However, in practice, a gap would form between the pipe and the soil at these two corners under the 'diagonal' loading condition which is examined in section 5.4. The highest peak value is in case SD2 and the peak value in case SD3 is much lower than those in the cases SD1 and SD2. The principal direction in the high stress region of $\theta = 90^0$ on the internal surface is similar in all three cases and is shown in Figure 5.5(d). The figure shows that the tensile stresses are mainly in the hoop direction at the pipe ends and the tensile direction changes to the normal direction of the line connecting the two loaded corners when towards to the middle length of the pipe.

Figure 5.6 shows the same normalized principal stresses in the concrete pipe with the pipe rotated 180 degrees in the θ direction. From the figure, it is clearly seen that the stress distribution patterns on the external surface of the pipe are quite different from those on the internal surface. Now the stress patterns are similar in all three cases, and the high stresses are located at the central area on the external surface and the two non-loaded corners (the reason for high stress at the non-loaded corners was discussed above for Figure 5.5) . Again, the highest stress is in the case SD2 and the peak value in case SD3 is much lower than those in the other two cases. Figure 5.6(d) shows the principal direction in the high stress regions (similar in all three cases). Again, the tensile stresses are in the hoop direction at the two non-loaded corners and in the normal direction of the line connecting the two loaded corners at the central area on the external surface.

The normalized most compressive principal stresses are shown in Figure 5.7. The figure shows that the high magnitudes of the stresses are located at the two diagonal loaded corners and there is a small band connecting these two corners with lower magnitudes of stress; and that the stress magnitudes reduce when away from the band towards the other two non-loaded corners. The change of the stress magnitude is small across the pipe thickness. The peak magnitudes are very similar to those under the corresponding 'edge' loading conditions.

5.4 INTERACTION BETWEEN THE PIPE AND THE SURROUNDING SOIL

To remove effect of unrealistic stresses acting on the external surface of the pipe from the surrounding soil as discussed in Section 5.3 and to study the interaction between the pipe and its surrounding soil, a layer of interface elements was used between the pipe and the soil in the analysis described in this section. For simplicity, the soil was also treated as linearly elastic with the same Poisson's ratio $\mu_s = 0.2$ and the same three different Young's moduli E_s = 144MPa, 14.4MPa and 1440MPa.

The interaction between the pipe and its surrounding soil was modelled by using the elastic perfectly-frictional Mohr-Coulomb model described in Chapter 2. In the second stage of research at Oxford about pipe jacking (Milligan and Norris 1993a, Norris 1992), it was found that the frictional angle between the pipe and its surrounding soil varied from 12^0 to 37^0 under different ground conditions and the cohesion parameter c was small. However, the analysis is not aimed at representing any particular ground condition in practice but to study the general effect of the interaction between the pipe and the surrounding soil. In the analysis, an arbitrary frictional angle $\phi = 15^0$ and an associated dilation angle $\psi = 15^0$ were used. A small cohesion parameter c = 0.05MPa was taken for the purpose of numerical stability in the analysis because there was no initial contact stresses between the pipe and the surrounding soil. The shear stiffness K_s and the normal stiffness K_n of the interface were

chosen according to the stiffness and dimensions of the soil in the model, that is, 50MPa /mm and 100MPa /mm for E_s =144 MPa, 5MPa /mm and 10MPa /mrn for E_s =14.4MPa, and 500MPa /mm and 1000MPa /mm for E_s =1440MPa.

The finite element mesh and the dimensions of the domain are shown in Figure 5.8(a) to 5.8(d), which are almost the same as those used in Section 5.3 except that there is a layer of interface elements between the pipe and its surrounding soil. The boundary conditions and the loading conditions are the same as those without the interface in Section 5.3. The solution method for the analysis described in this section is the initial stiffness method due to the difficulties with the modified Euler method. (When the modified Euler iteration procedure was used in the analysis with this model, the convergence was very slow and the unbalanced force was large, especially under the diagonal loading condition.) The total numbers of calculation steps were 400 for the 'edge' loading case and 500 for the 'diagonal' loading case. Within each calculating step, there were several iterations depending on the convergent condition while the maximum number of iterations was 10.

5.4.1 EDGE LOADING WITH INTERFACE ELEMENTS

This section describes the analysis with the 'edge' load and with three cases FE1, FE2 and FE3 for the same three different soil stiffness. The normalized normal stresses on the unfolded interface in case FE1, FE2 and FE3 are shown in Figure 5.9(a), 5.9(b) and 5.9(c) respectively. From the figure, it is clear that the stress patterns in all three cases are similar and that the high magnitudes of the normal stresses are at the two corners in the region of $\theta = 180^0$. However, the peak magnitudes are small in case FE1 and FE2. In case FE3, the peak magnitude of the normalized normal stresses is about 0.45.

The normalized shear stresses on the unfolded interface in case FE1, FE2 and FE3 are shown in Figure 5.10(a), 5.10(b) and 5.10(c) respectively. Clearly, the shear stress patterns

on the interface in all three cases are similar to those of the normal stresses. The normalized stresses are concentrated at the two corners in the region of $\theta = 180^0$ and the peak values are small except in case FE3. (It should be pointed out that the stresses in the soil might be beyond the soil strength under both 'edge' and 'diagonal' loading, especially in the case of soft soil. The soil plasticity is discussed in Section 5.5 with the modified Matsuoka model. If a lubricant is used in pipe jacking, the friction between the pipe and the soil will reduce significantly.)

From the discussion above, it is clear that the pipe is separated or almost separated from the surrounding soil over most of the external surface. However, the effect of the distribution of the stresses from the surrounding soil on the stresses in the pipe are believed to be small since the magnitudes of the stresses on the interface are small except in the case FE3.

The normalized most tensile principal stresses in the pipe are shown in Figure 5.11(a), 5.11(b) and 5.11(c) for case FE1, FE2 and FE3 respectively. The figure shows that the stress distributions and the peak values of the tensile stresses are similar to those in the case without interface elements in Section 5.3.1. The difference between the stresses with stiff soil in Figure 5.11(c) and those in Figure 5.11(a) and 5.11(b) is due to the reaction stresses from the soil on the interface as discussed above. The principal direction in the regions with high tensile stresses is also similar to that in Section 5.3.1 (refer to Figure 5.3(d)). Similar comments are applied to the normalized most compressive principal stresses in the concrete pipe which are not discussed in detail here (refer to Section 5.3.1, and see Figure 5.4).

5.4.2 DIAGONAL LOADING WITH INTERFACE ELEMENTS

Under the 'diagonal' loading condition, again, three calculation cases, FD1, FD2 and FD3, for the same three different soil stiffnesses have been studied. The normalized normal stresses on the unfolded interface under the 'diagonal' load are given in Figure 5.12(a),

5.12(b) and 5.12(c) for case FD1, FD2 and FD3 respectively. From the figure, it is clearly seen that in all three cases the distribution patterns of the normal stresses on the unfolded interface are similar and the stresses are concentrated at the two diagonal loaded corners, and that the stresses on the other two corners and central area are almost zero. The highest stress magnitude is in case FD3 while the peak magnitudes in case FD1 and FD2 are slightly lower.

The normalized shear stresses on the unfolded interface under the 'diagonal' load are given in Figure 5.13(a), 5.13(b) and 5.13(c) for case FD1, FD2 and FD3. Again, the shear stresses are concentrated in the two diagonal loading corners. The stresses at the two non-loaded diagonal corners are zero and the stresses at the central area are very small. The highest stress is also in case FD3 with the highest soil Young's modulus.

The results of the normal and shear stresses on the interface clearly suggest that the pipe is separated from its surrounding soil at the two non-loaded diagonal corners and is almost separated at the central area of the external surface while the pipe is supported by the surrounding soil at the two diagonal loaded corners.

The normalized most tensile principal stresses in the pipe under the 'diagonal' load are shown in Figure 5.14, with the stresses in case FD1 in Figure 5.14(a), the stresses in case FD2 in Figure 5.14(b) and the stresses in case FD3 in Figure 5.14(c). The figure shows that in case FD1 and FD2 the stress patterns are similar, but they are quite different from those without interface elements in Section 5.3, and that the tensile stresses on the external surface of the pipe at the two non-loaded corners in Figure 5.5 vanished due to the gap between the pipe and the soil as discussed above. The stresses are concentrated on the internal surface of the pipe near the non-loaded corners and the stresses at the two diagonal loaded corners are almost zero. In the case FD3, the high stresses are in the central area on the internal surface while its peak stress is much lower than those in the other two cases due to the higher reaction stresses from the soil as discussed above. The highest stress is in case FD2 with the

soft soil. The principal direction in the high stress regions is somewhat similar for all three cases and is shown in Figure 5.14(d). In general, the tensile stresses are in the hoop direction in the region of $\theta = 180^0$ and 0^0, and change towards to the normal direction of the line connecting the two loaded corners when moving towards to the central region of $\theta = 90^0$.

Figure 5.15 shows the normalized most tensile principal stresses in the pipe under the 'diagonal' load viewed from the opposite direction. The stresses on the external surface of the pipe are very high at the central area and the stresses at the two loaded corners are almost zero as on the internal surface. The peak values are higher than those on the internal surface with the highest stress still in case FD2. The tension direction at the central area of the external pipe surface is mainly in the normal direction of the line connecting the two loaded corners in all three cases as shown in Figure 5.15(d).

The normalized most compressive principal stresses in the pipe under the 'diagonal' loading condition are shown in Figure 5.16. From the figure, it is clear that the stress patterns are similar to those without the interface elements in Section 5.3.2 except that the peak magnitudes are slightly higher (see Figure 5.7).

5.5 ANALYSIS WITH PLASTIC SOIL

In this section, a further analysis with plastic surrounding soil without the interface is described. In general, the yielding behaviour of the soil is dependent on the type of soil (Das 1983, Bolton 1979). For example, von-Mises' model is appropriate to describe the behaviour of clays under undrained conditions, and the Matsuoka model and Mohr-Coulomb model with a high frictional angle are suitable for sands. In the analysis described in this section, the soil was modelled by the elastic perfectly-plastic Matsuoka model described in Chapter 2. One thing that should be stressed here is that the plastic model is not intended to describe any particular soil in practice. Rather, the analyses were carried out to study the effect of the

surrounding soil in which frictional behaviour was important, as pointed out in Section 5.4. To enable the soil model to describe the friction between the pipe and the surrounding soil and to perform some functions of an interface, the material parameters of the soil were chosen to be the same as those used for the interface model in Section 5.4, that is, the triaxial frictional angle $\phi = 15^{\circ}$, the triaxial dilation angle $\psi = 15^{\circ}$, the soil cohesion c = 0.05MPa, the Poisson's ratio $\mu_s = 0.2$ and the three different Young's moduli. (It should be pointed out that the dilation angle of the soil is defined as $\tan\psi = \frac{d\varepsilon_v}{d\gamma}$, where $d\varepsilon_v$ and $d\gamma$ are the volumetric strain and shear strain in the soil shear test (Atkinson 1993). However, in the current research, only the friction of the soil was considered and an associated flow rule was used. In the modified Matsuoka model, the plastic potential was assumed to be the same as the yield function, that is, $\psi = \phi$ (see Section 2.4.2).) In the analysis described in this section, the solution method was also the initial stiffness method described in Chapter 2. The total numbers of calculation steps were 400 for the 'edge' loading case and 500 for the 'diagonal' loading case. Again, within each calculating step, there were several iterations depending on the convergent condition.

5.5.1 EDGE LOADING WITH PLASTIC SOIL

The finite element mesh, boundary condition and the loads were the same as those shown in Figure 5.1 and 5.2 in Section 5.3.1. Again, three cases (PE1, PE2 and PE3) with the same three different Young's moduli of the surrounding soil E_s = 144MPa, 14.4MPa and 1440MPa were included in the analysis.

The normalized most tensile principal stresses in the pipe under 'edge' loading with the plastic surrounding soil are shown in Figure 5.17. The figure shows that in all three cases the tensile stress distributions are almost same as those with the elastic surrounding soil in Sections 5.3 and 5.4. The peak value in case PE3 is higher than that in case E3 and FE3 although it is still much lower than those in case PE1 and PE2. The principal direction in the

high stress regions is mainly in the hoop direction in all three cases as discussed in Section 5.3 (see Figure 5.3(d)). As for the most compressive stresses in the pipe, the distribution patterns and the peak magnitudes are also the same as those with the corresponding elastic surrounding soil, and are not discussed here in detail (refer to the discussion in Section 5.3.1 and see Figure 5.4).

5.5.2 DIAGONAL LOADING WITH PLASTIC SOIL

Under the 'diagonal' loading case and with the plastic surrounding soil, the three calculation cases are called PD1, PD2 and PD3 with the same three different Young's moduli of the surrounding soil E_s = 144MPa, 14.4MPa and 1440MPa. All other conditions were unchanged from those in the cases with the elastic surrounding soil in Section 5.3.2.

Figure 5.18 shows the normalized most tensile principal stresses in the pipe under the 'diagonal' loading with the plastic surrounding soil. The stress distributions in all three cases are similar to those in case FD1 and FD2 in Section 5.4.2 except that the centres of the high stresses are slightly further away from the two non-loaded corners and the high stress domains extend further towards the pipe centre in the θ direction. The peak value of the stress in case PD3 is much higher than that in case FD3 in Section 5.4.2 and SD3 in Section 5.3.2 although it is still lower than those in case FD1 and FD2 . The principal direction in the high stress regions is also similar in all three cases and shown in Figure 5.18(d). Again, the tension is mainly in the hoop direction in the region of $\theta = 180^0$ and 0^0, and changes towards the normal direction of the line connecting the two loaded corners when moving towards the central region of $\theta = 90^0$.

Figure 5.19 shows the most tensile principal stresses in the pipe under the 'diagonal' load with the plastic surrounding soil with the pipe rotated 180 degrees in the θ direction. The figure shows that the stress patterns are similar in all three cases and that the stresses are

highly concentrated at the central areas on the external surface of the pipe as in the case with interface except that the peak stresses are higher than the corresponding ones in Section 5.4.2, especially in the case PD3. Similar to the case with interface in Section 5.4, in all three cases the tension at the central area of the external pipe surface is mainly in the normal direction of the line connecting the two loaded corners as shown in Figure 5.19(d).

As for the normalized most compressive principal stresses in the pipe under the 'diagonal' load with the plastic surrounding soil, both the distribution patterns and the peak magnitudes of the stress are very similar to those shown in Figure 5.16 in Section 5.4.2 and it is not discussed any further about them here (refer to Section 5.4.2 and see Figure 5.16).

5.6 CONCLUSION

This chapter describes the analyses of the numerical model B with elastic surrounding soil, interface elements between the pipe and its elastic surrounding soil and plastic surrounding soil under both the 'edge' load and the 'diagonal' load. In all cases, the stress distributions are complex three-dimensional patterns as found in Chapter 4. In general, under the 'edge' load, high tensile stresses are located near the loading border at the pipe joint and the compressive stresses are concentrated at the loaded corners; under the 'diagonal' load, the high tensile stresses are in two domains near the diagonal loaded corners on the internal surface and at the central area on the external surface, and the compressive stresses are also concentrated at the loaded corners.

After analyzing the results from the numerical model B in this chapter, some conclusions about the behaviour of the pipe with its surrounding soil are reached as follows:

(1) Under the 'edge' load, the effect of the interaction between the pipe and soil, and the plasticity of the surrounding soil is very small; while under the 'diagonal' load, the effect of the interaction and the plasticity of the surrounding soil is significant.

(2) Under the same loading condition, the surrounding soil tends to reduce the tensile stresses in the pipe under both the 'edge' and the 'diagonal' loading condition, especially with a very stiff surrounding soil.

(3) Pipe testing under 'diagonal' loading without soil surrounding the pipe may give incorrect results due to the interaction between the pipe and the soil.

(4) The tensile stresses in the concrete pipe could be more important than the compressive stresses during pipe jacking due to the misalignment of the pipeline and the low tensile strength of the concrete which is usually one tenth of its compressive strength (Jiang and Feng 1991, Neville 1981).

(5) The 'diagonal' loading condition seems to be more severe than the 'edge' loading condition since the tensile stresses in the pipe are higher and over a wider region under the 'diagonal' loading condition.

(6) The results suggest that the surrounding soil has removed the local constraint effect under the 'diagonal' loading condition found in Chapter 4, and that both the interface and the plastic surrounding soil have eased the unrealistic tensile stresses acting on the external surface of the pipe from the surrounding soil.

5.7 BACK ANALYSIS OF NORRIS' EXPERIMENTAL DATA

In the second stage of the Oxford research on pipe jacking, Norris (1992) carried out monitoring of field behaviour of pipes at full scale on five active construction sites. In his research, the loading distribution at the pipe joint was measured using pressure cells glued to the pipe ends. The measured load distributions of case BA1 and BA2 and the location of the pressure cells on site 5 are shown in Figure 5.20(a) and 5.20(b) respectively. Furthermore, average strains on the internal surface of the pipe were measured by using tube extensometers which were of 1600mm gauge length and located at the middle part of the pipe. An analysis was carried out by Norris (1992) taking the pipe as a stocky column subject to axial load and biaxial bending as shown in Figure 5.21(a) and 5.21(b) for case BA1 and BA2 respectively.

Since in both cases the change of the bending moment along the pipe length is very small (less than one percent), Norris calculated the analytical strains at the section of z = 1250mm instead of the average ones. In the numerical analysis, since the strains were calculated at Gauss points, the numerical strains were calculated on a surface r = constant very near the internal surface of the pipe instead of on the internal surface.

In the back analysis, a full scale concrete pipe and the surrounding soil were used as shown in Figure 5.22. The three-dimensional mesh is shown in Figure 5.22(a); the surface of r = constant unfolded on a plane is shown in Figure 5.22(b); the section of z = constant in Figure 5.22(c) and the section of $\theta = 0^0$ in Figure 5.22(d). The dimensions of the pipe are the same as those of the full scale pipe used by Norris in his experiment. The dimensions of the pipe and of the domain are also shown in Figure 5.22(d). For the boundary condition, the nodes on the external surface of the domain were all fixed in both x and y directions. The applied load was assumed to be constant across the thickness of the pipe since the pressure cells on the pipe end spanned across the full pipe thickness and to have the same distribution patterns in θ direction as the measured data shown in Figure 5.20. The total applied load on the pipe end was P = 4525kN and P = 3640kN for case BA1 and BA2 respectively. The assumed distributed loads on the external surface of the pipe were ignored in the analysis since the surrounding soil was included to deal with the interaction between the pipe and the surrounding soil. The distributions of applied load showed that it was an 'edge' load, and that the load was over half the cross section of the pipe. So both the concrete pipe and the surrounding soil were treated as linear elastic in the analysis (refer to the conclusion in Section 5.6). The material constants were the same as those used by Norris (1992) in his research, that is, the Young's modulus E_c = 40000MPa and the Poisson's ratio μ_c = 0.2 for the concrete pipe, and the Young's modulus E_s = 144MPa and the Poisson's ratio μ_s = 0.2 for the surrounding soil.

The average microstrains in the z direction over 1600mm in the middle part of the pipe on the internal surface (r = 600mm) are given in Figure 5.23(a) and 5.23(b) for cases BA1 and BA2 respectively. In the figure, the y axis is the microstrain and the x axis is θ in degrees. From the figure, it is clear that in case BA1 the numerical results, the measured values and the analytical results agree well with each other except that the analytical results deviate slightly when the strains are small and tensile in the region of $\theta = 180^0$. In case BA2, the agreement between the numerical results, the measured values and the analytical results are also good except that there is some deviation with the measured value in the region of $\theta = 150^0$, and with the analytical results in the regions of $\theta = 210^0$ and $\theta = 330^0$.

The results above suggest that both the numerical model B and the stocky column model are capable of obtaining reliable results for the average compressive strains in the middle part of the pipe under the 'edge' loading condition. However, one thing should be stressed here is that the stocky column model cannot gain accurate predictions at the pipe joint due to strain concentrations at the joint and lack of changes of the bending moment in the stocky column model; and that there is no similar simple analytical model for 'diagonal' loading.

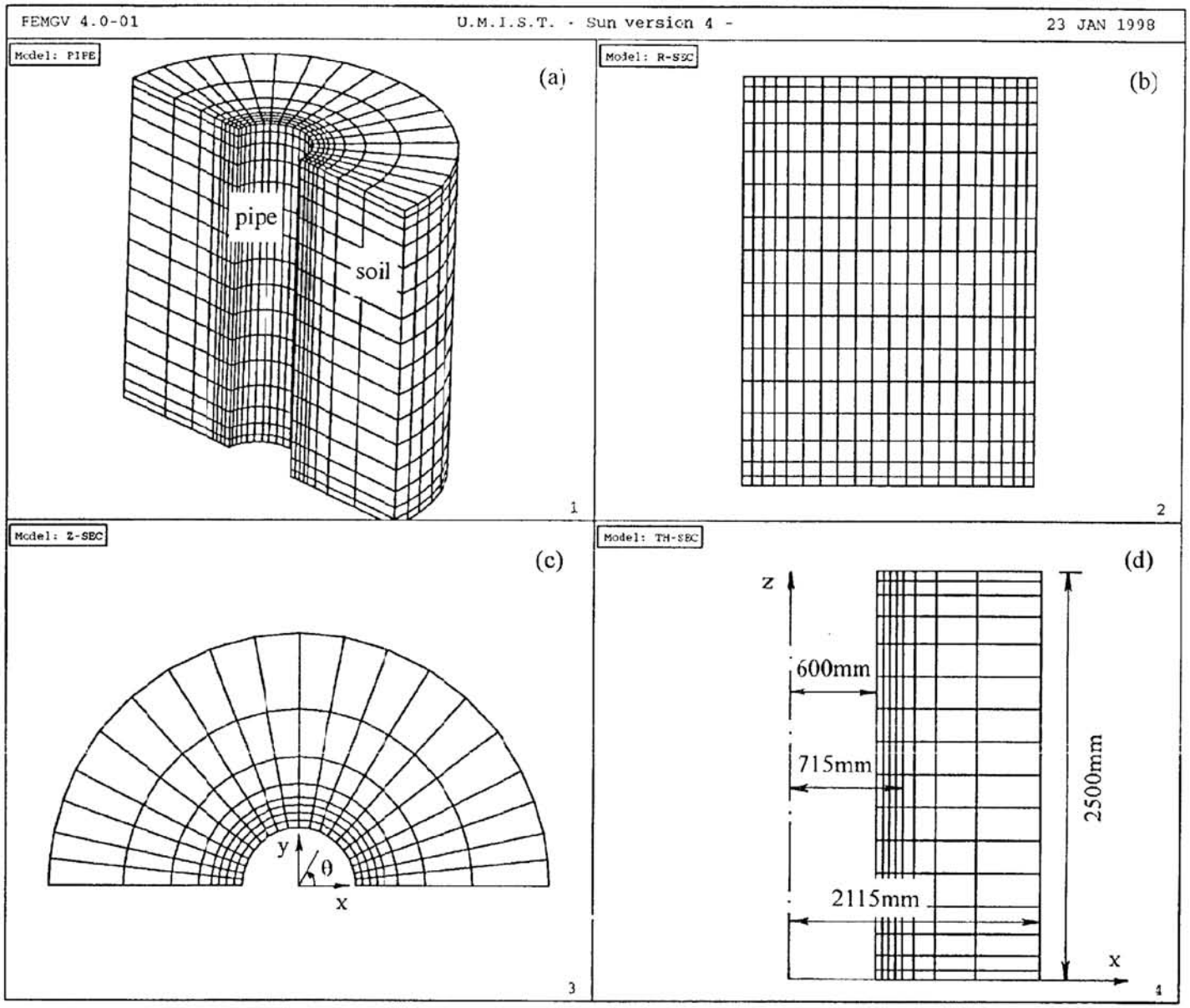


Figure 5.1 Numerical model B and its FE mesh

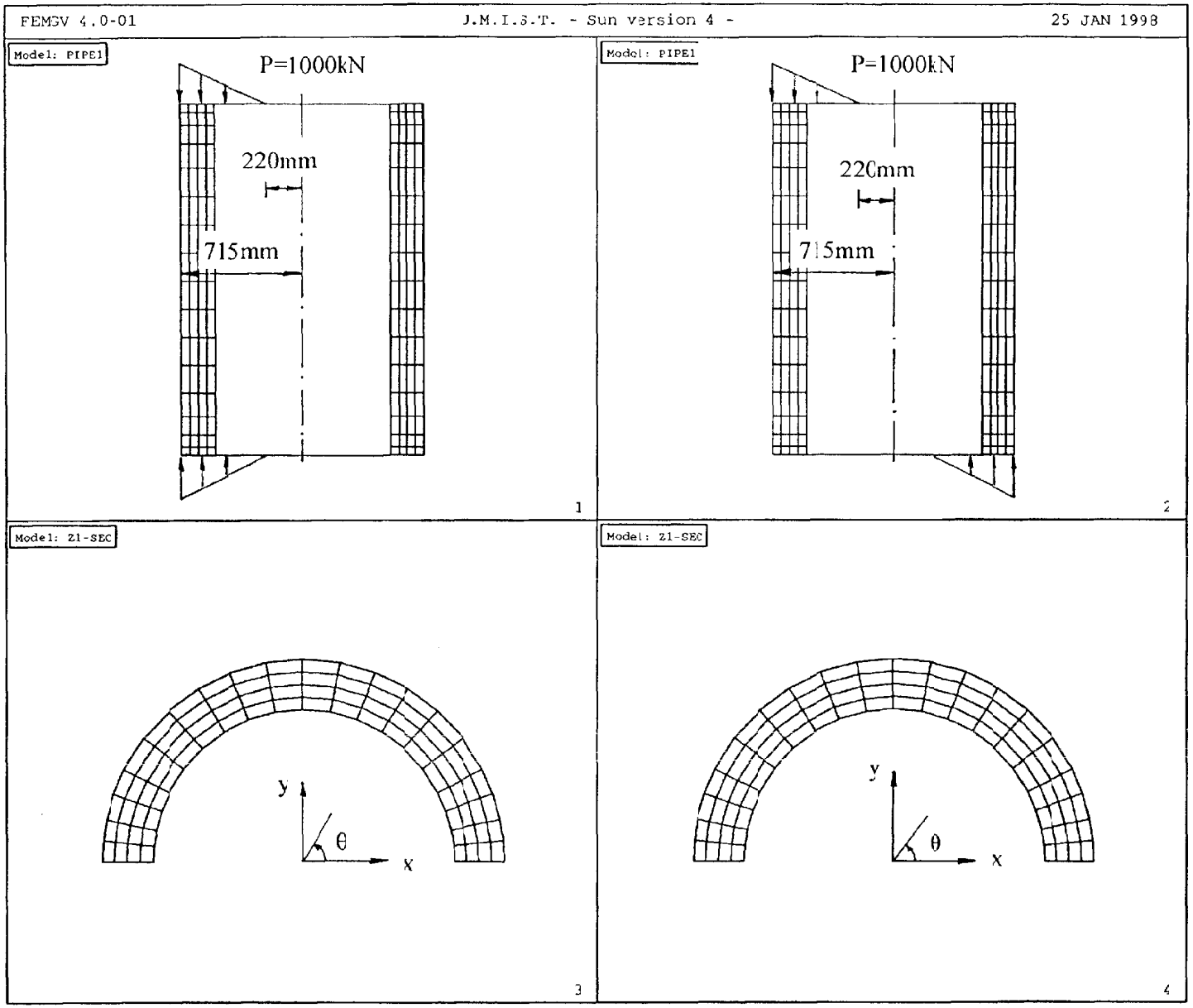


Figure 5.2 'Edge' load and 'diagonal' load

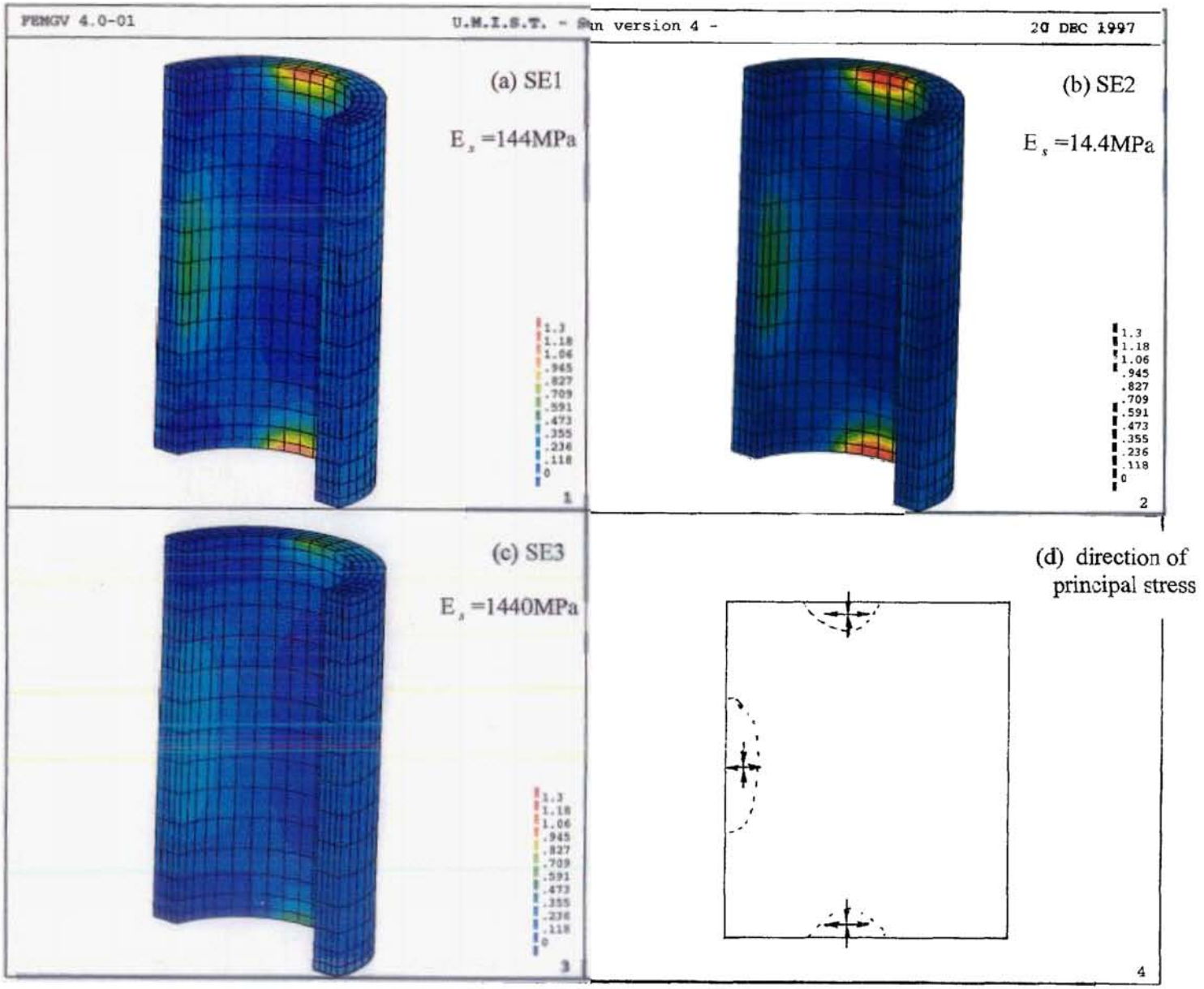


Figure 5.3 Normalized most tensile principal stresses in the pipe under 'edge' loading with elastic soil

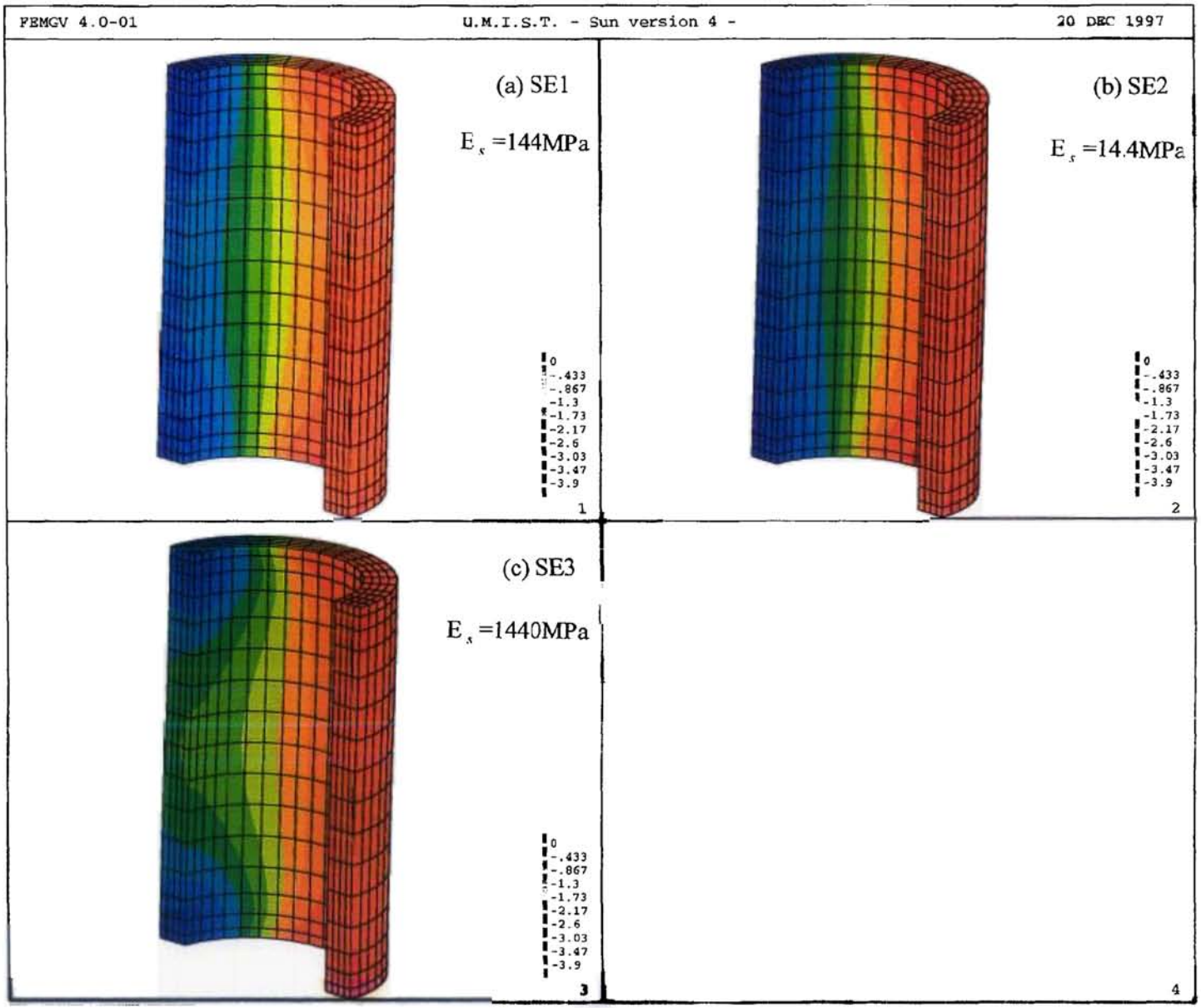


Figure 5.4 Normalized most compressive principal stresses in the pipe under 'edge' loading with elastic soil

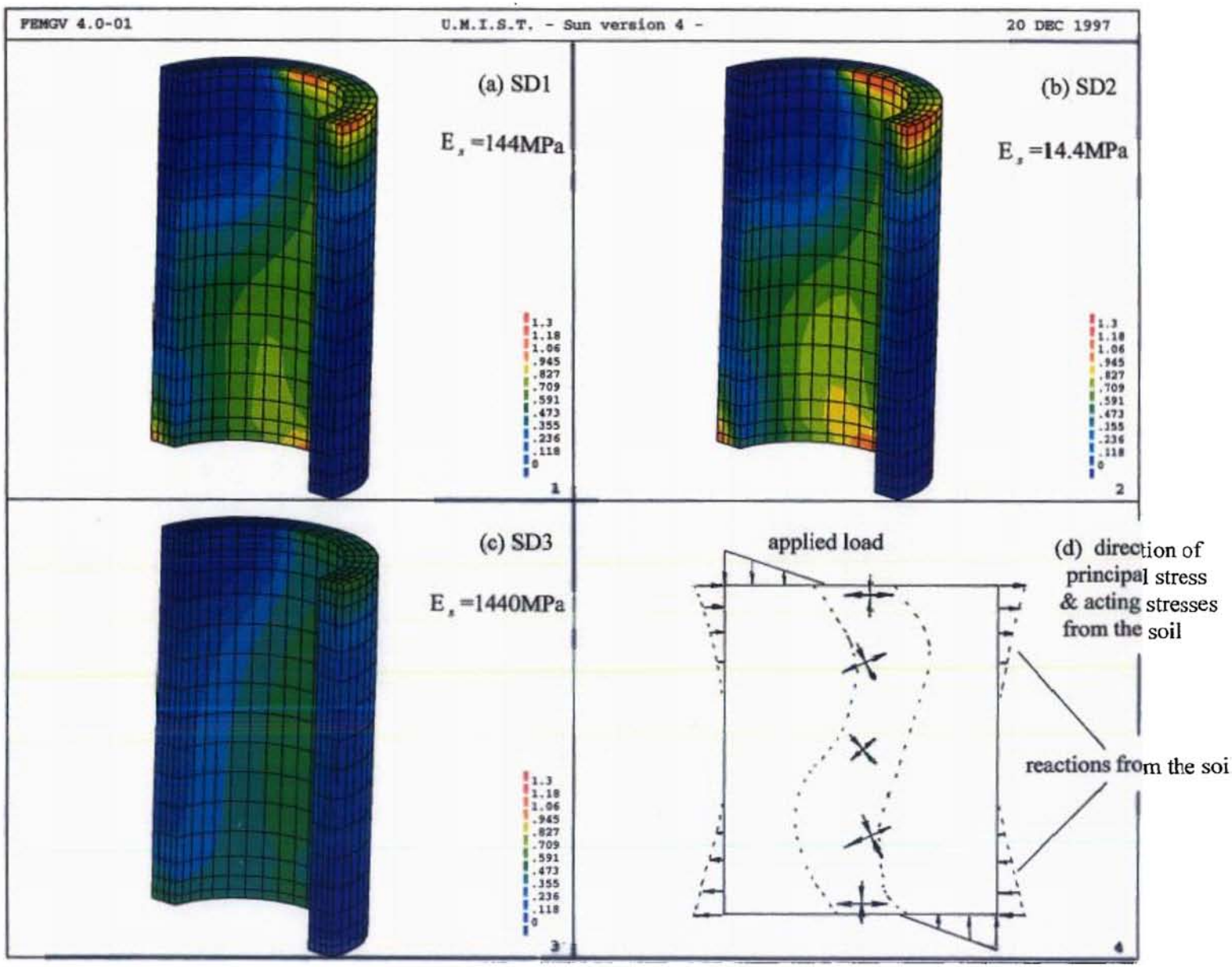


Figure 5.5 Normalized most tensile principal stresses in the pipe under 'diagonal' loading with elastic soil

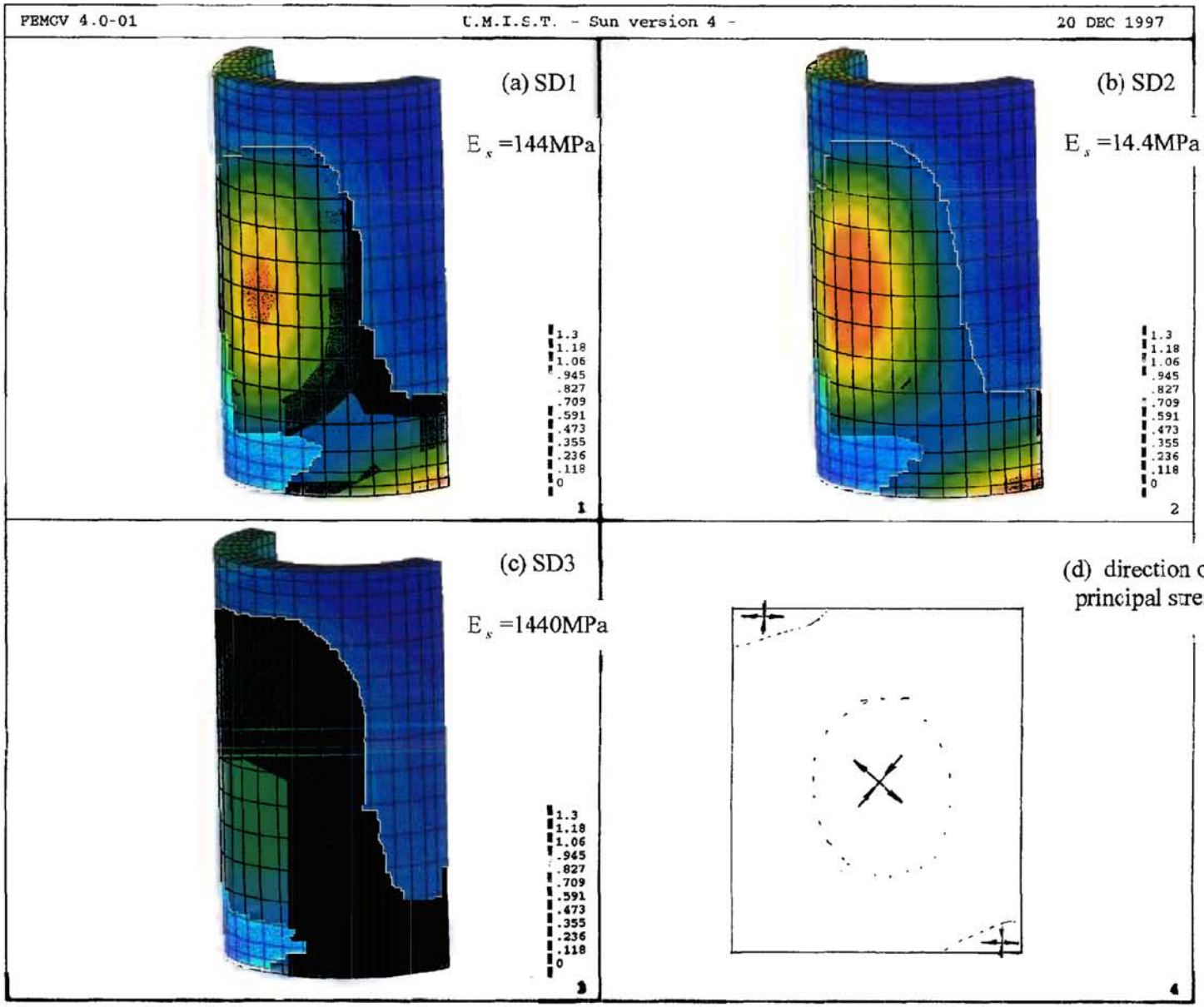


Figure 5.6 Normalized most tensile principal stresses in the pipe under 'diagonal' loading with elastic soil by looking from opposite direction

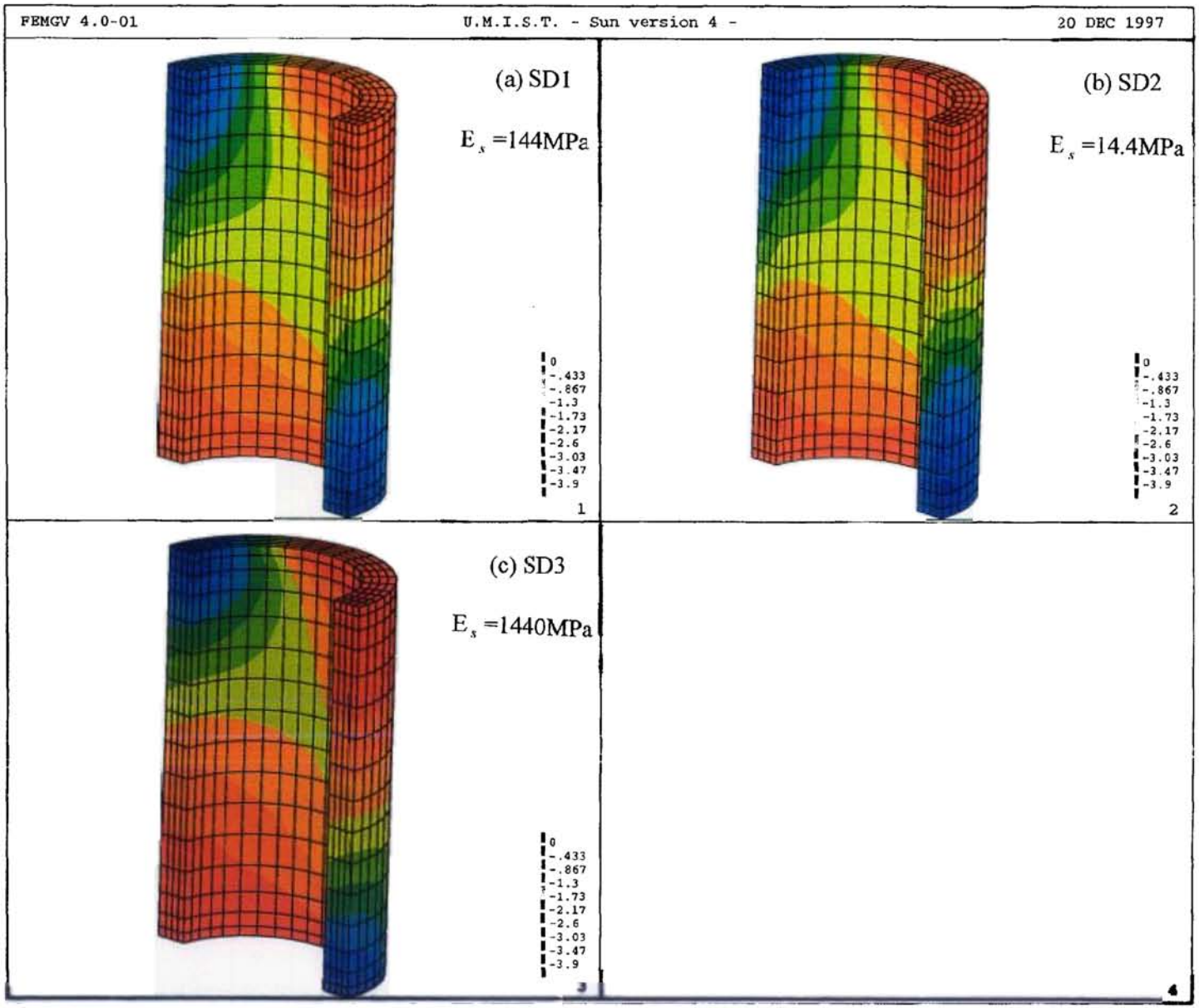


Figure 5.7 Normalized most compressive principal stresses in the pipe under 'diagonal' loading with elastic soil

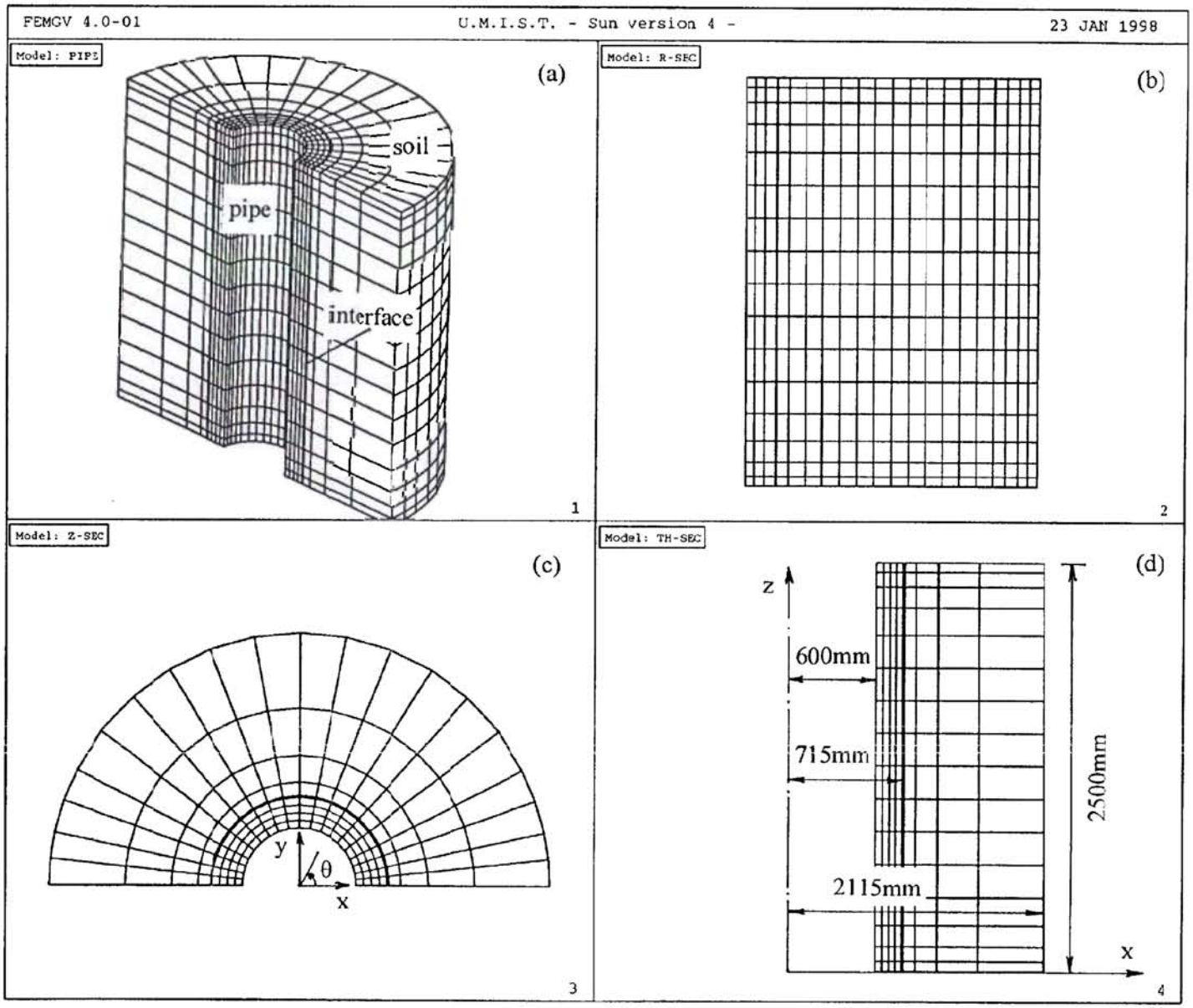


Figure 5.8 FE mesh of numerical model B with interface elements

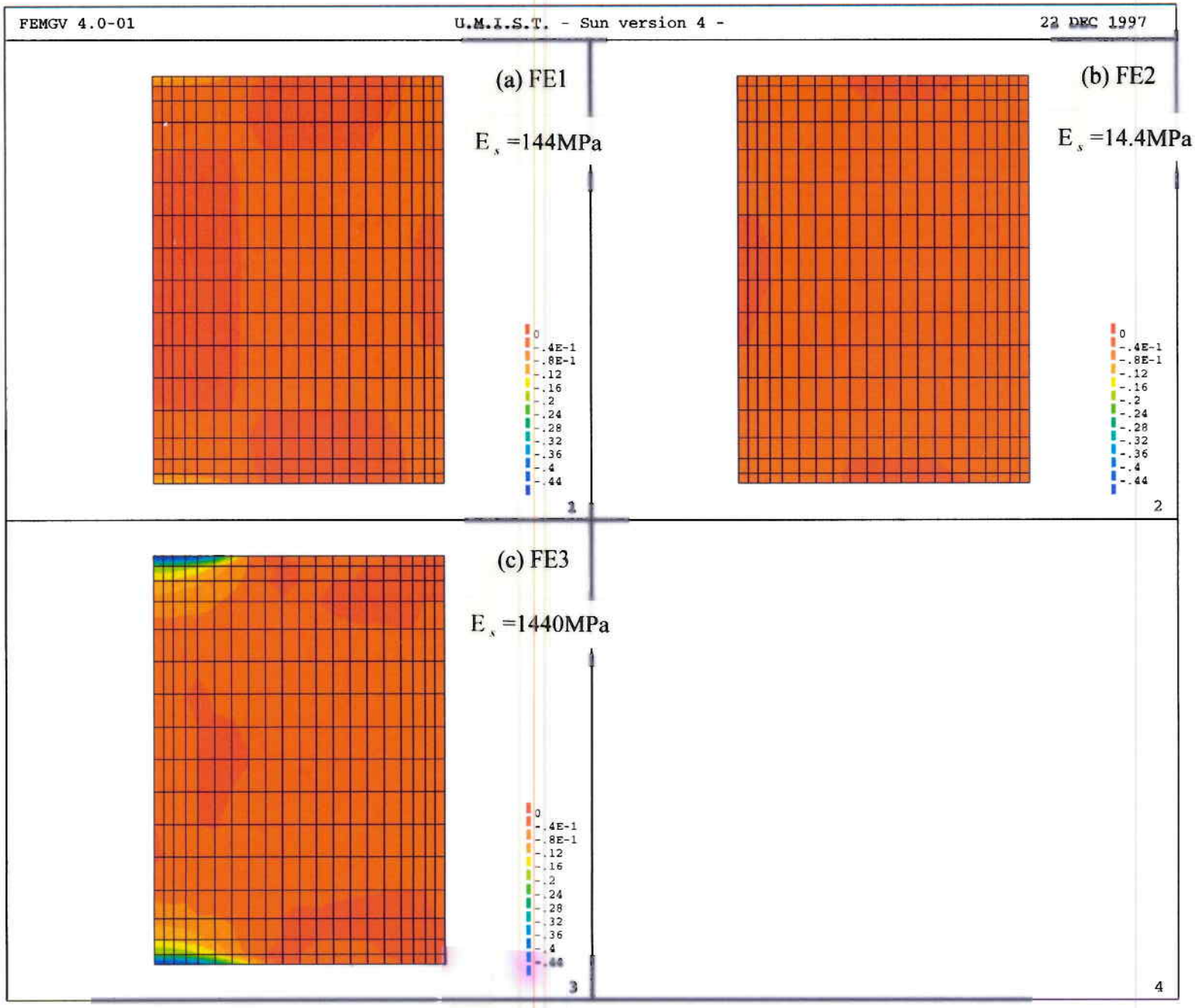


Figure 5.9 Normalized normal stresses on the unfolded interface under 'edge' loading

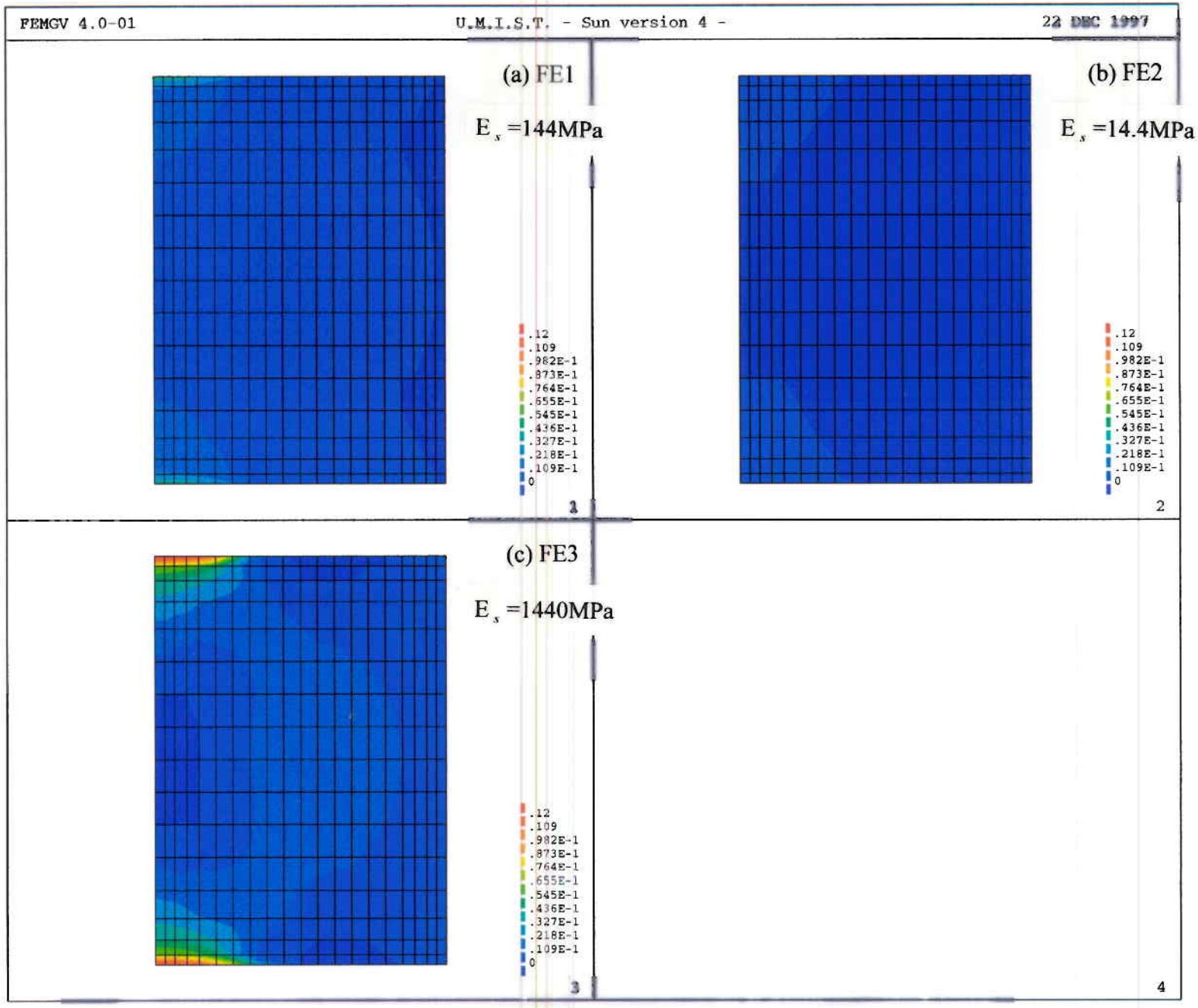


Figure 5.10 Normalized shear stresses on the unfolded interface under 'edge' loading

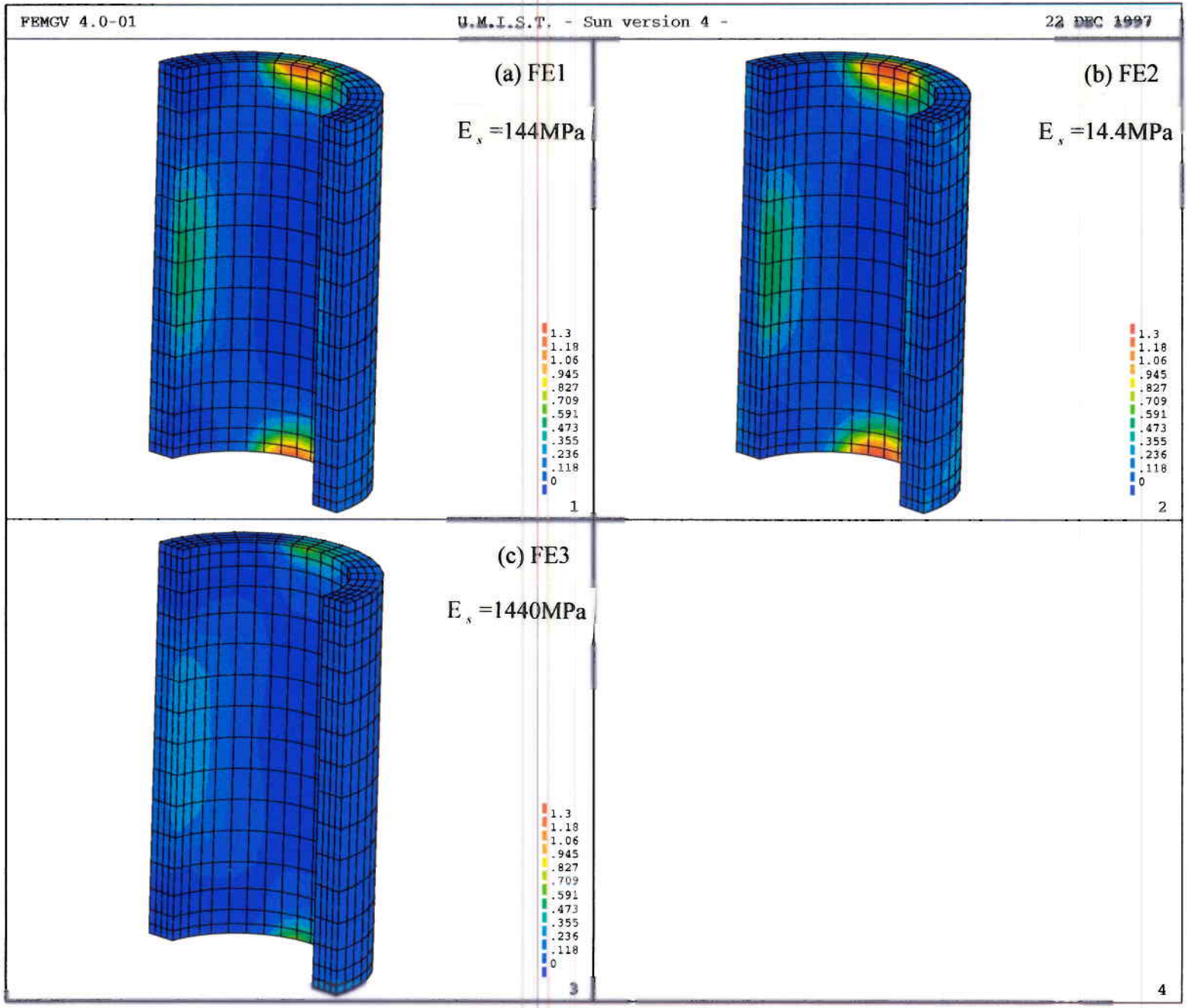


Figure 5.11 Normalized most tensile principal stresses in the pipe under 'edge' loading with interface

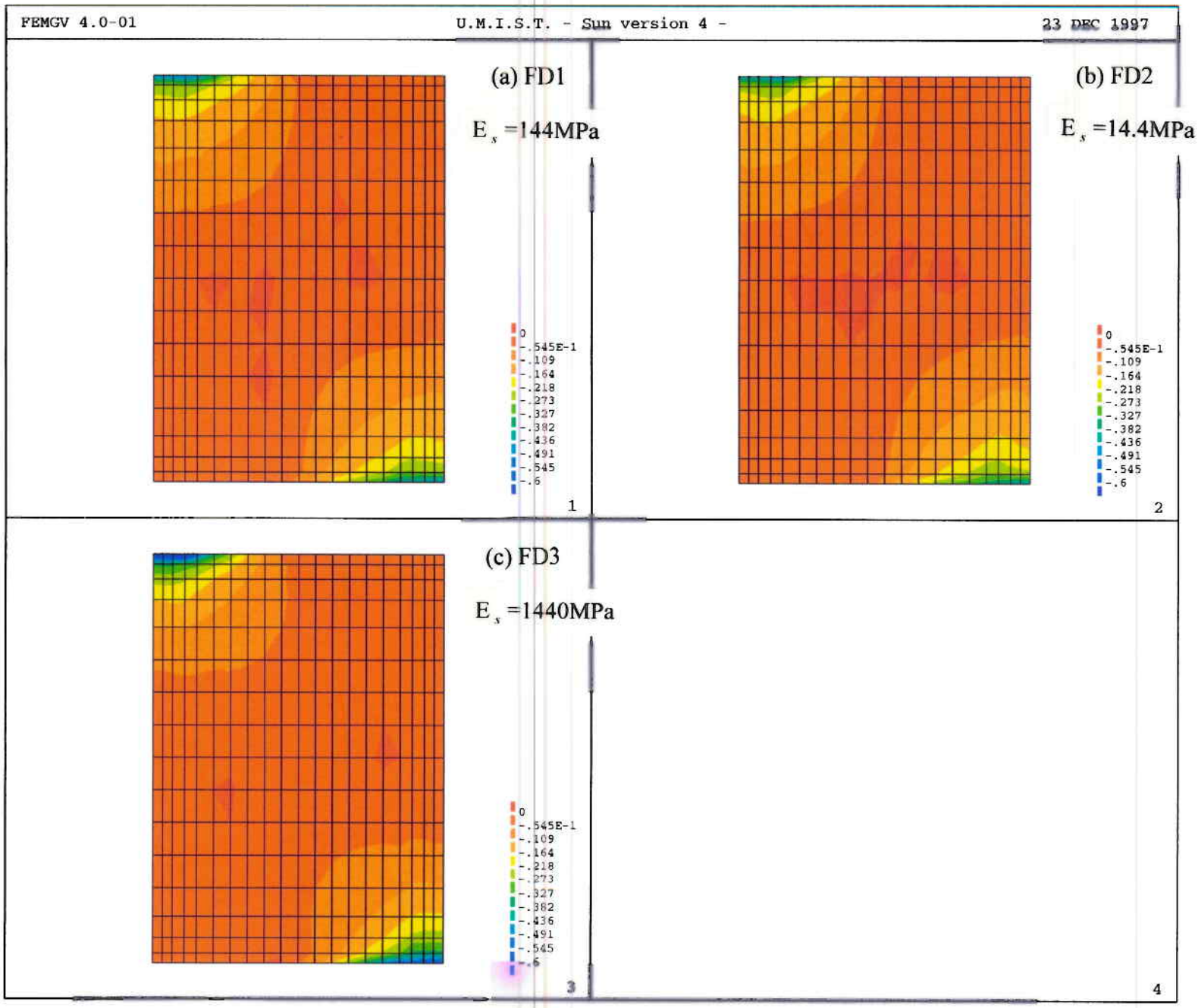


Figure 5.12 Normalized normal stresses on the unfolded interface under 'diagonal' loading

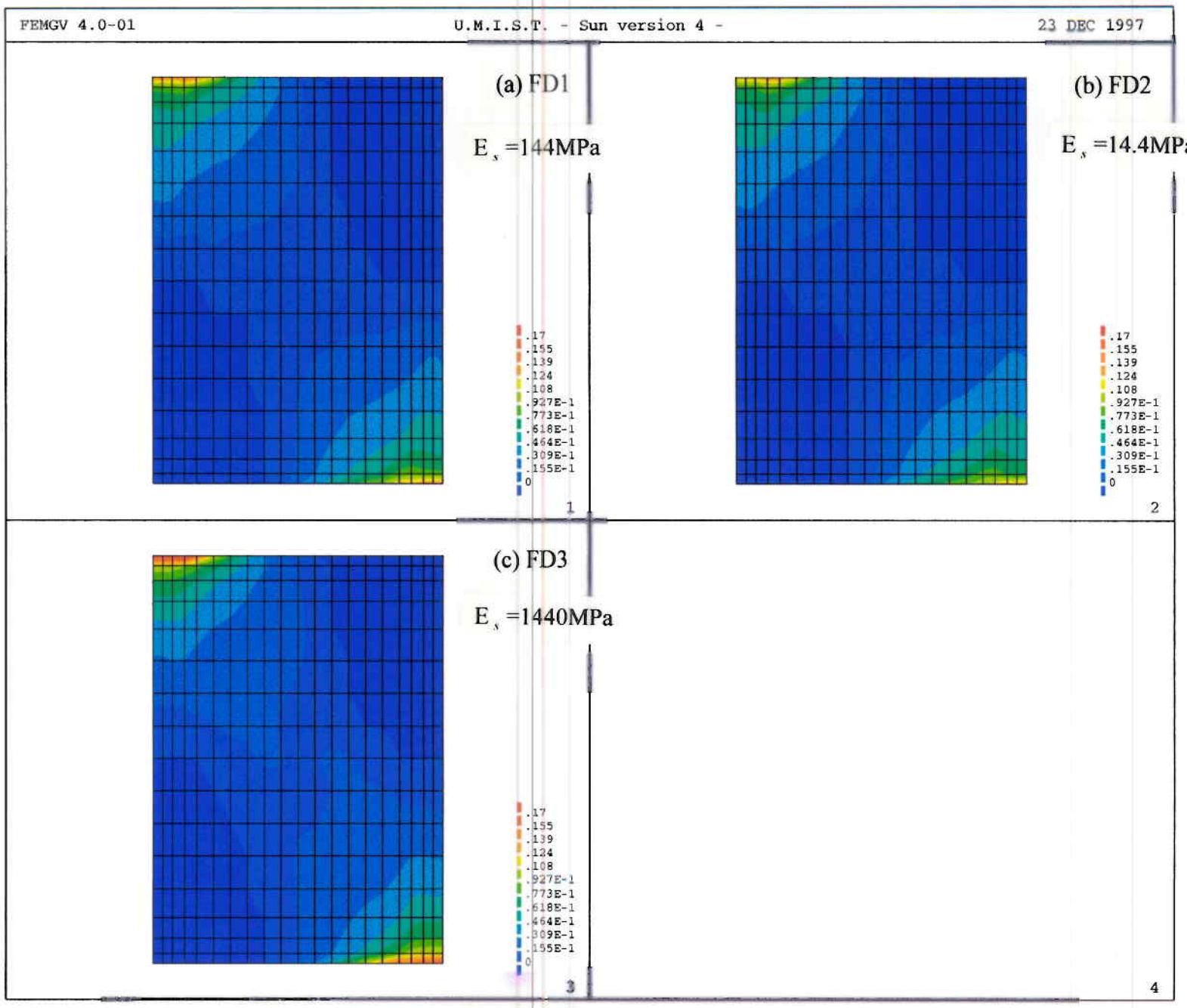


Figure 5.13 Normalized shear stresses on the unfolded interface under 'diagonal' loading

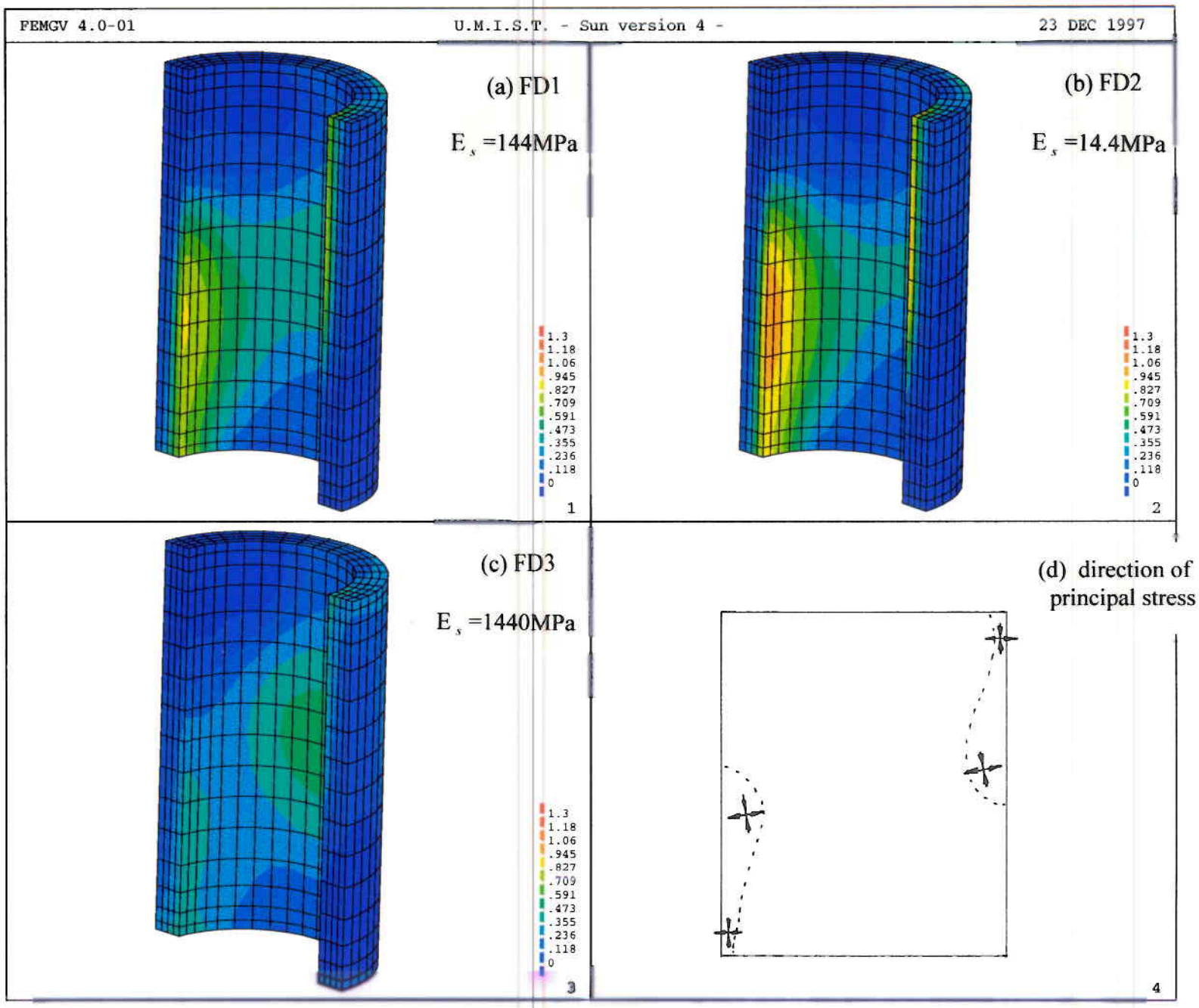


Figure 5.14 Normalized most tensile principal stresses in the pipe under 'diagonal' loading with interface

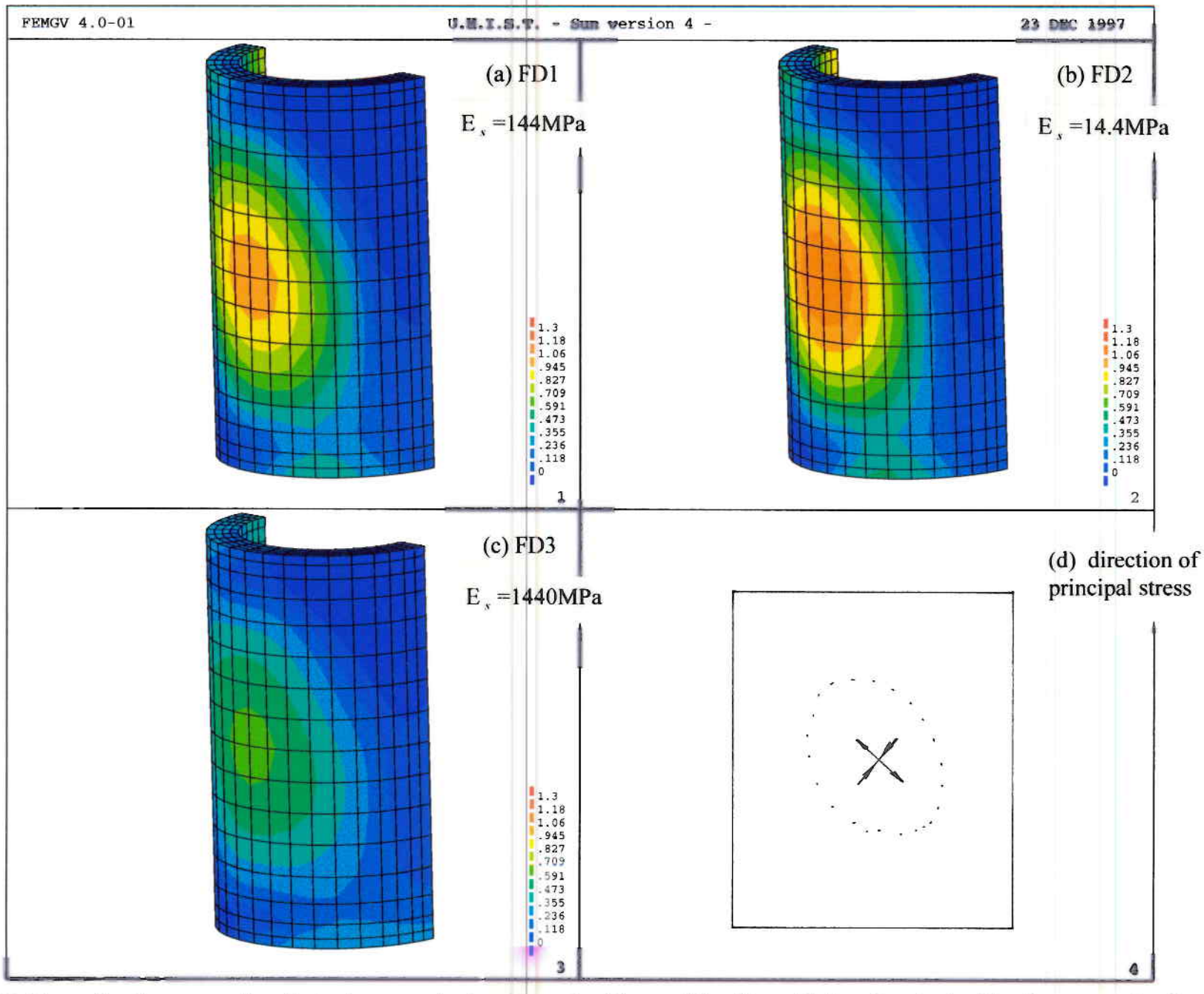


Figure 5.15 Normalized most tensile principal stresses in the pipe under 'diagonal' loading with interface by looking from opposite direction

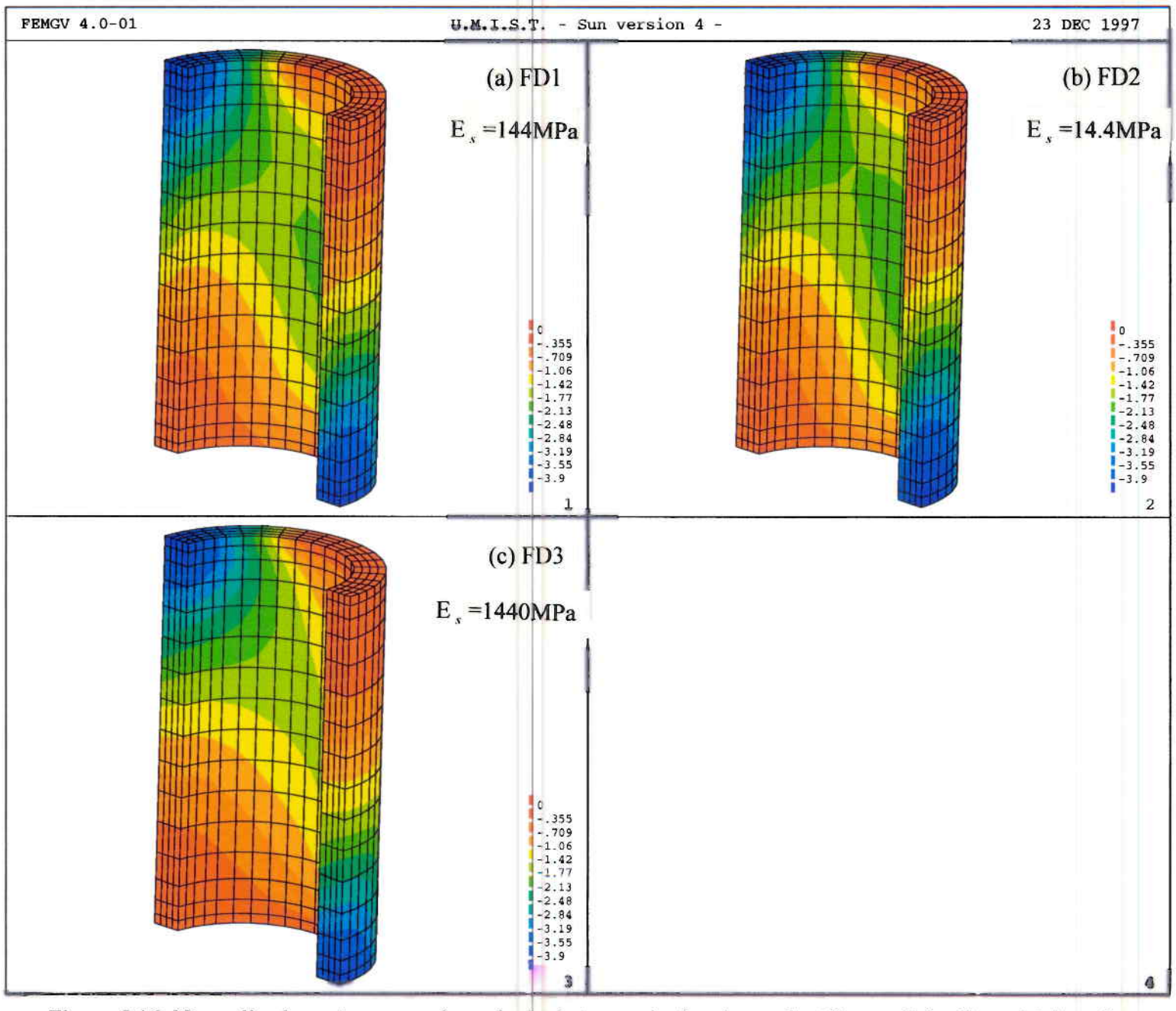


Figure 5.16 Normalized most compressive principal stresses in the pipe under 'diagonal' loading with interface

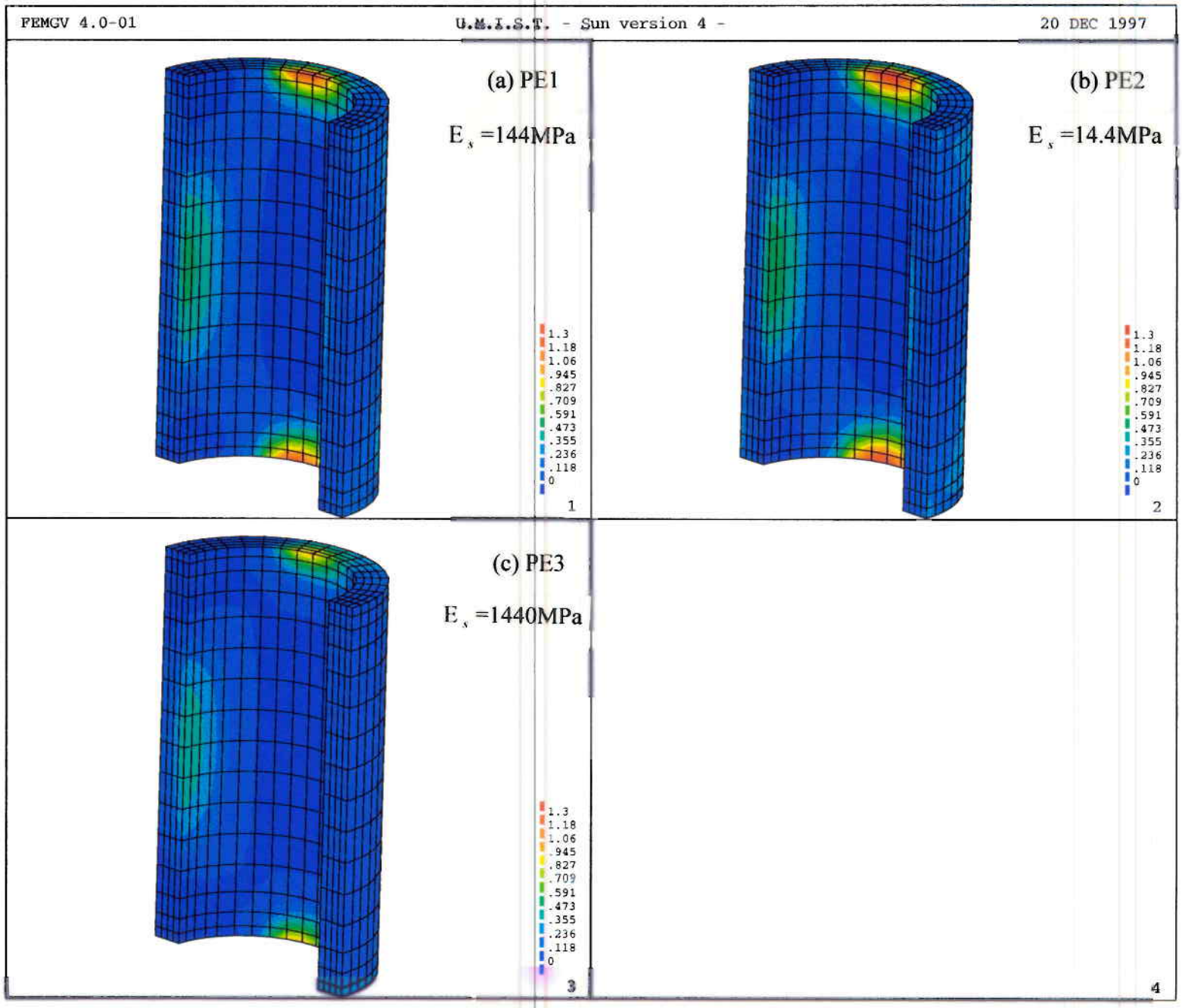


Figure 5.17 Normalized most tensile principal stresses in the pipe under 'edge' loading with plastic soil

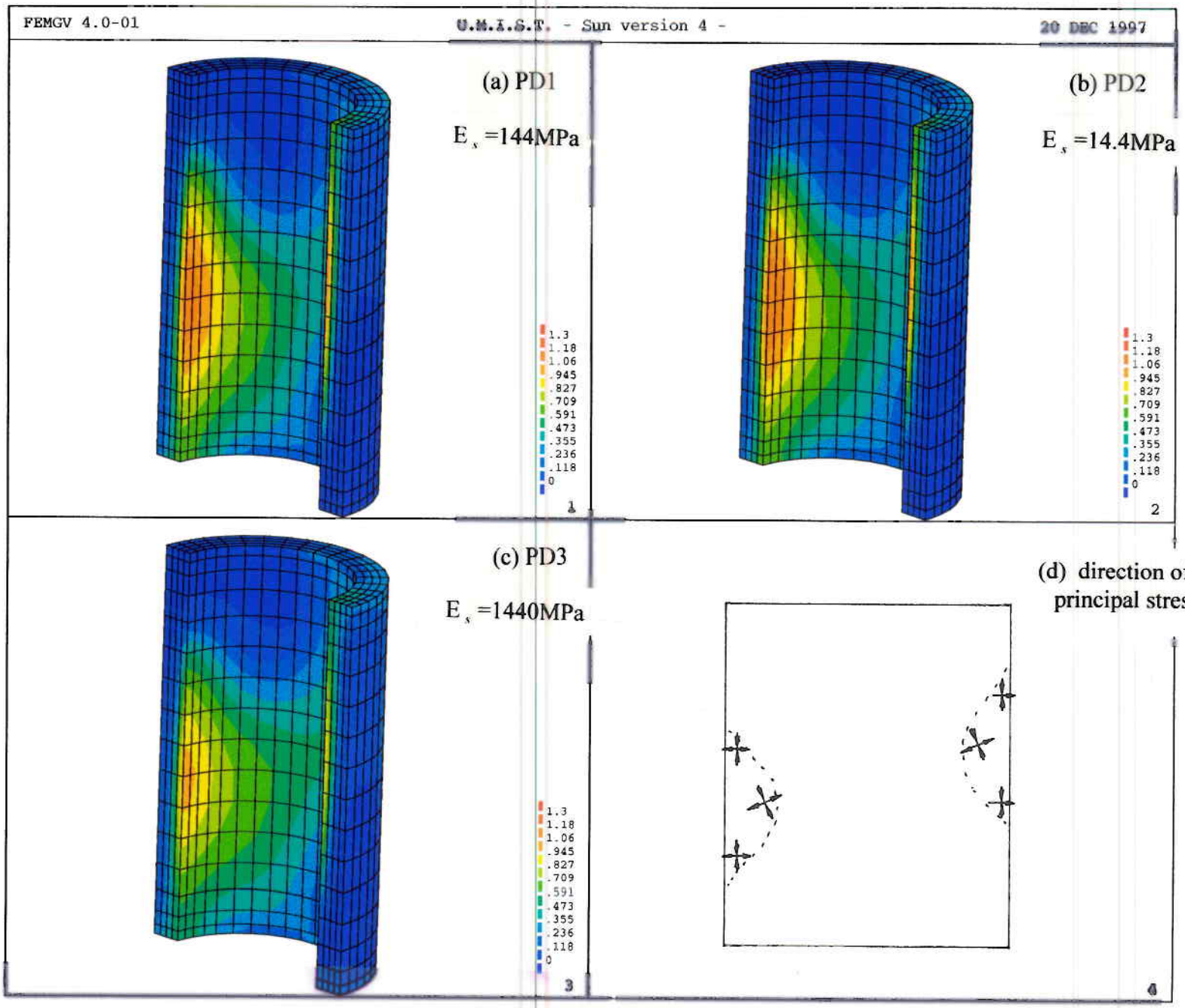


Figure 5.18 Normalized most tensile principal stresses in the pipe under 'diagonal' loading with plastic soil

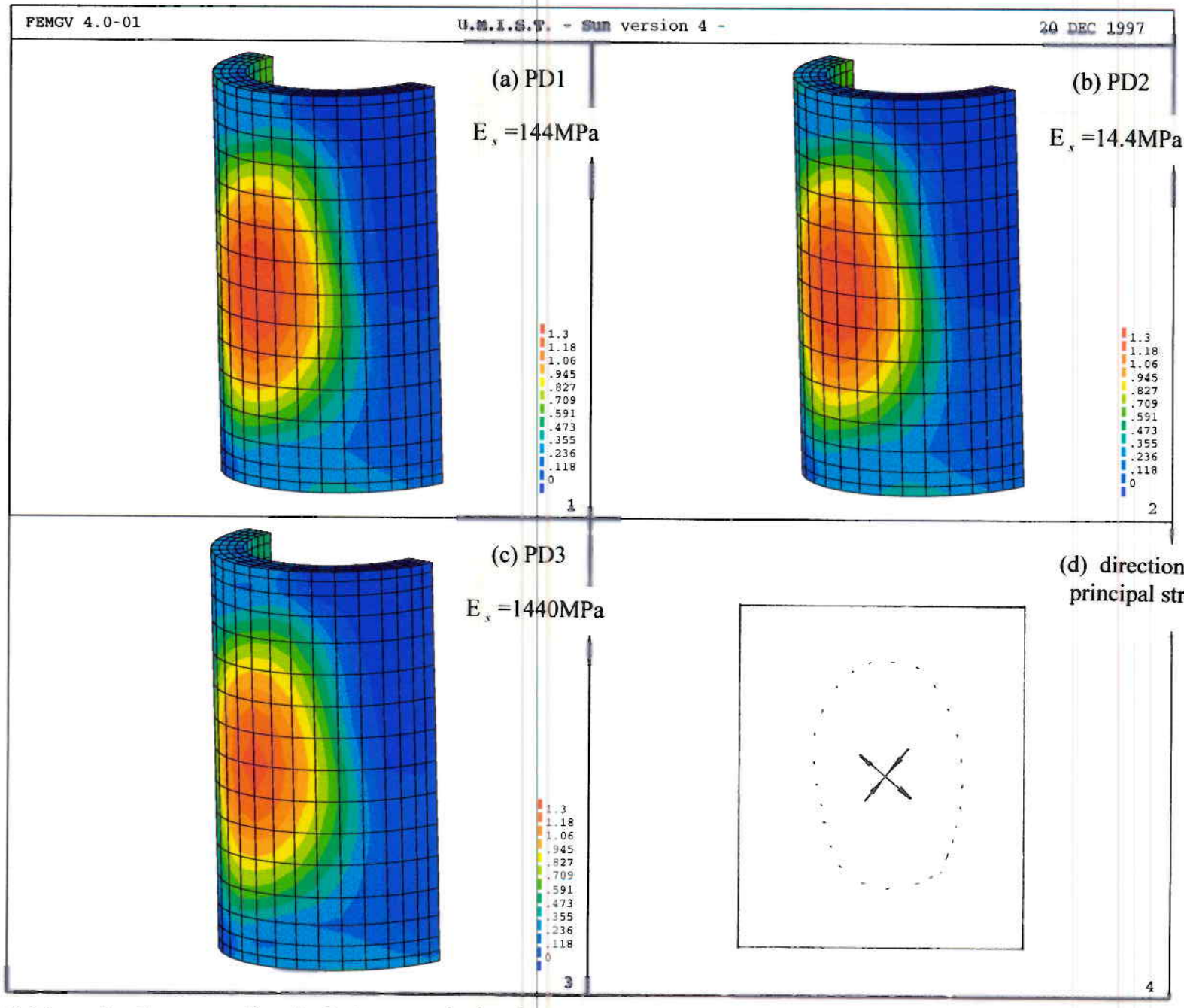


Figure 5.19 Normalized most tensile principal stresses in the pipe under 'diagonal' loading with plastic soil by looking from opposite direction

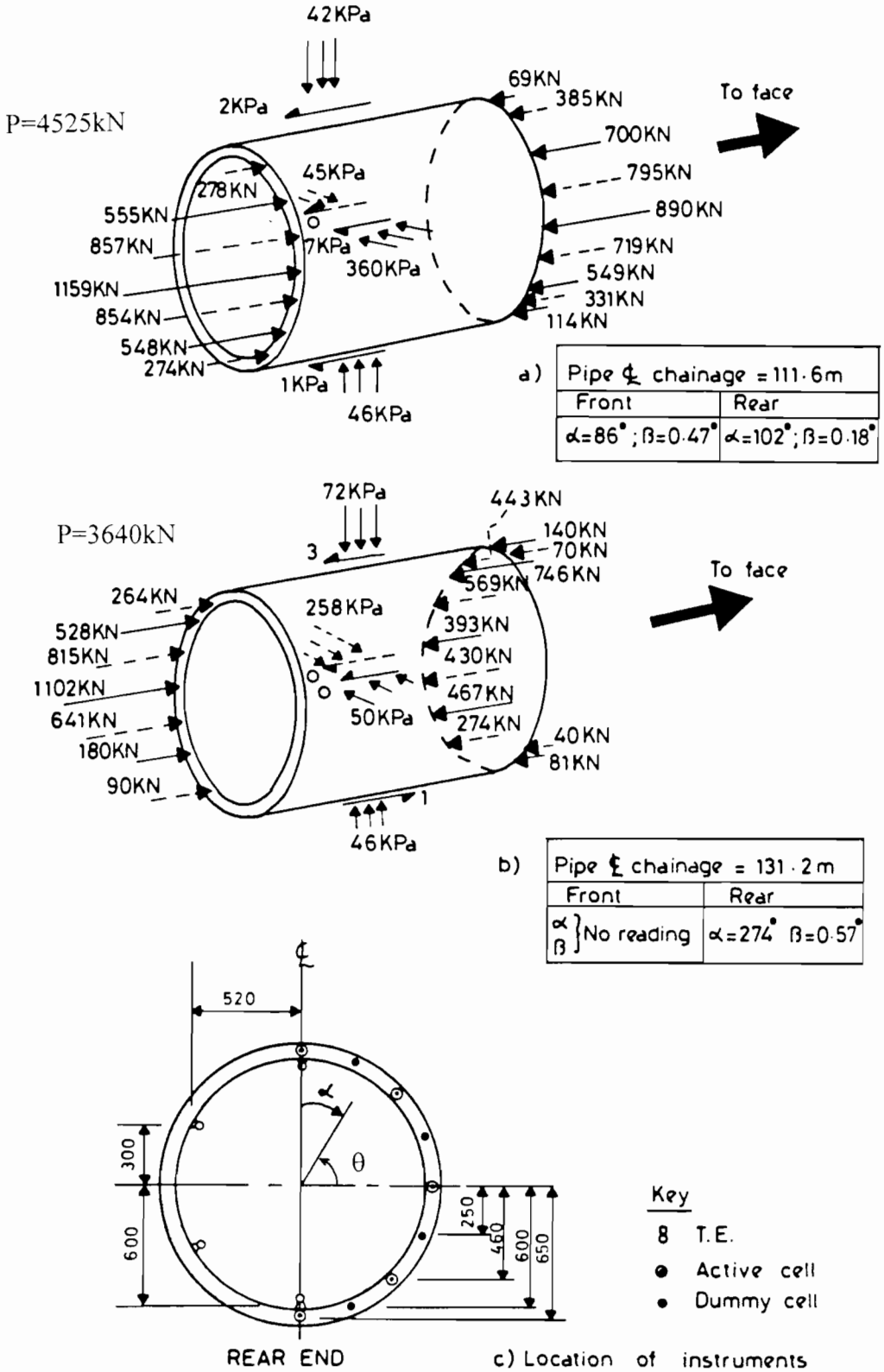
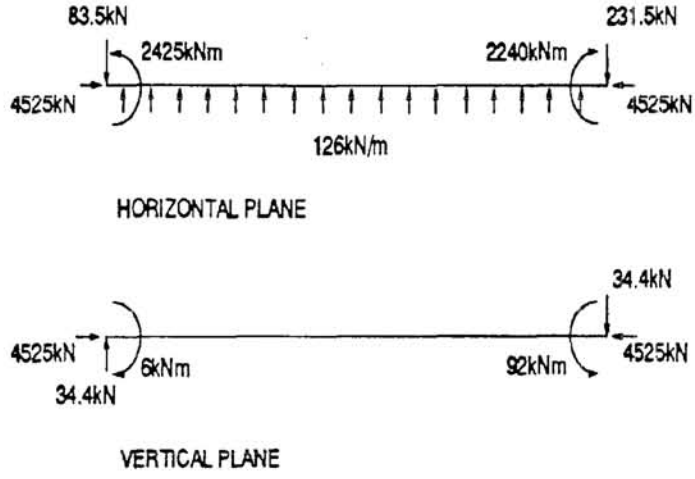
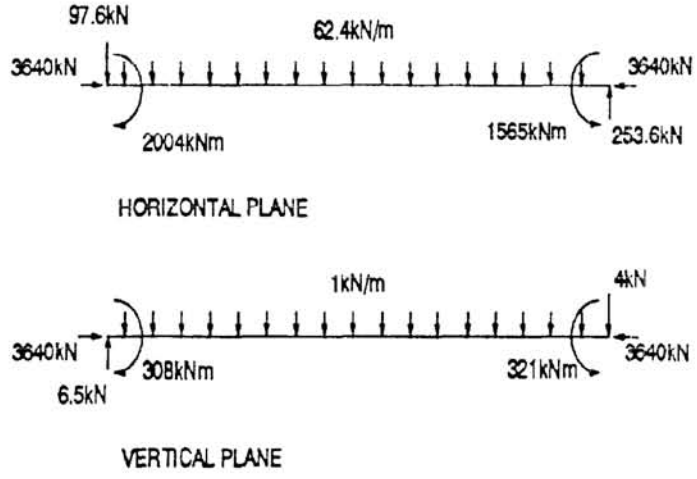


Figure 5.20 Measured load distribution at pipe joint (from Norris 1992)



(a) BA1



(b) BA2

Figure 5.21 Stocky column model (from Norris 1992)

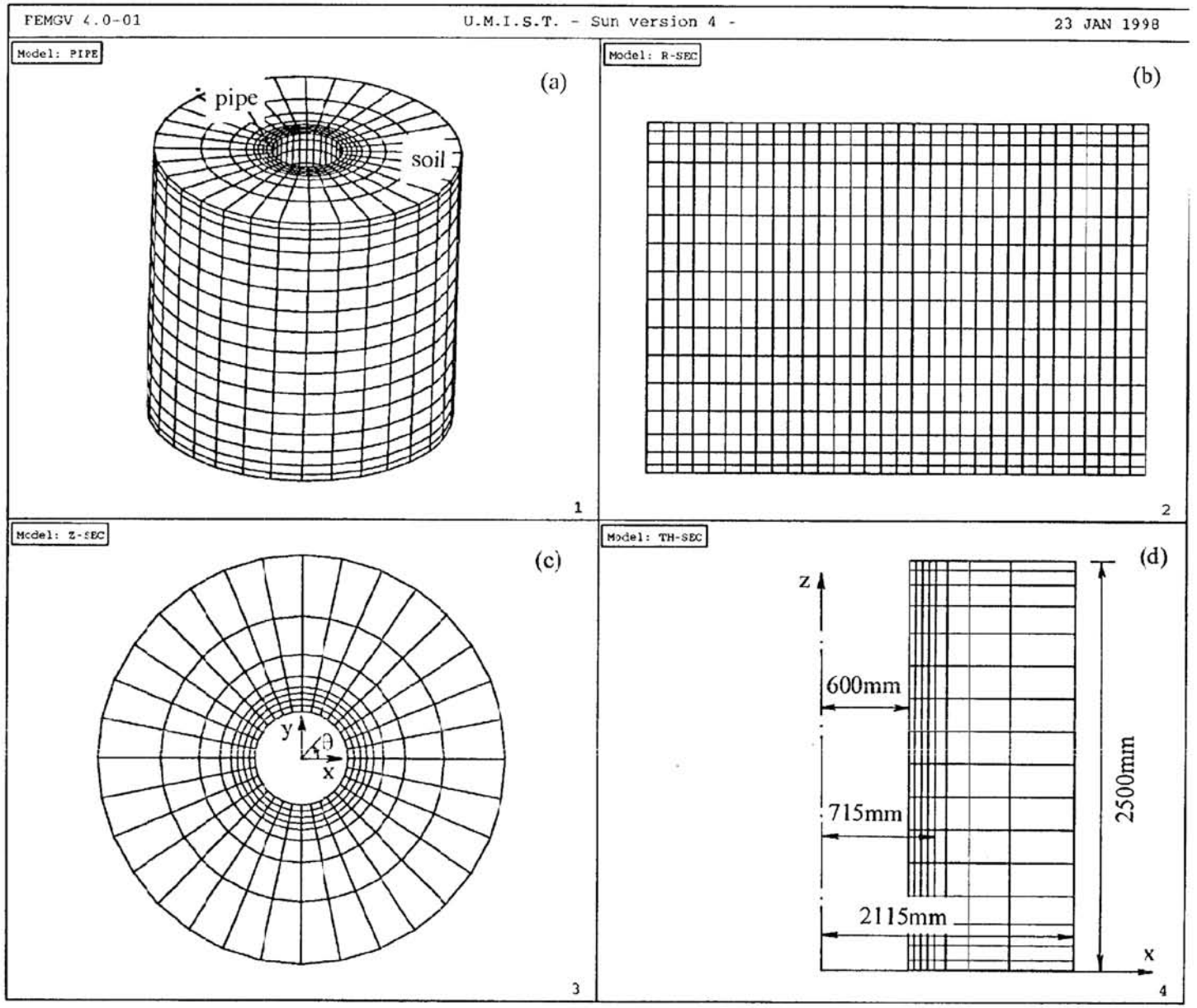


Figure 5.22 FE mesh of numerical model B for back analysis

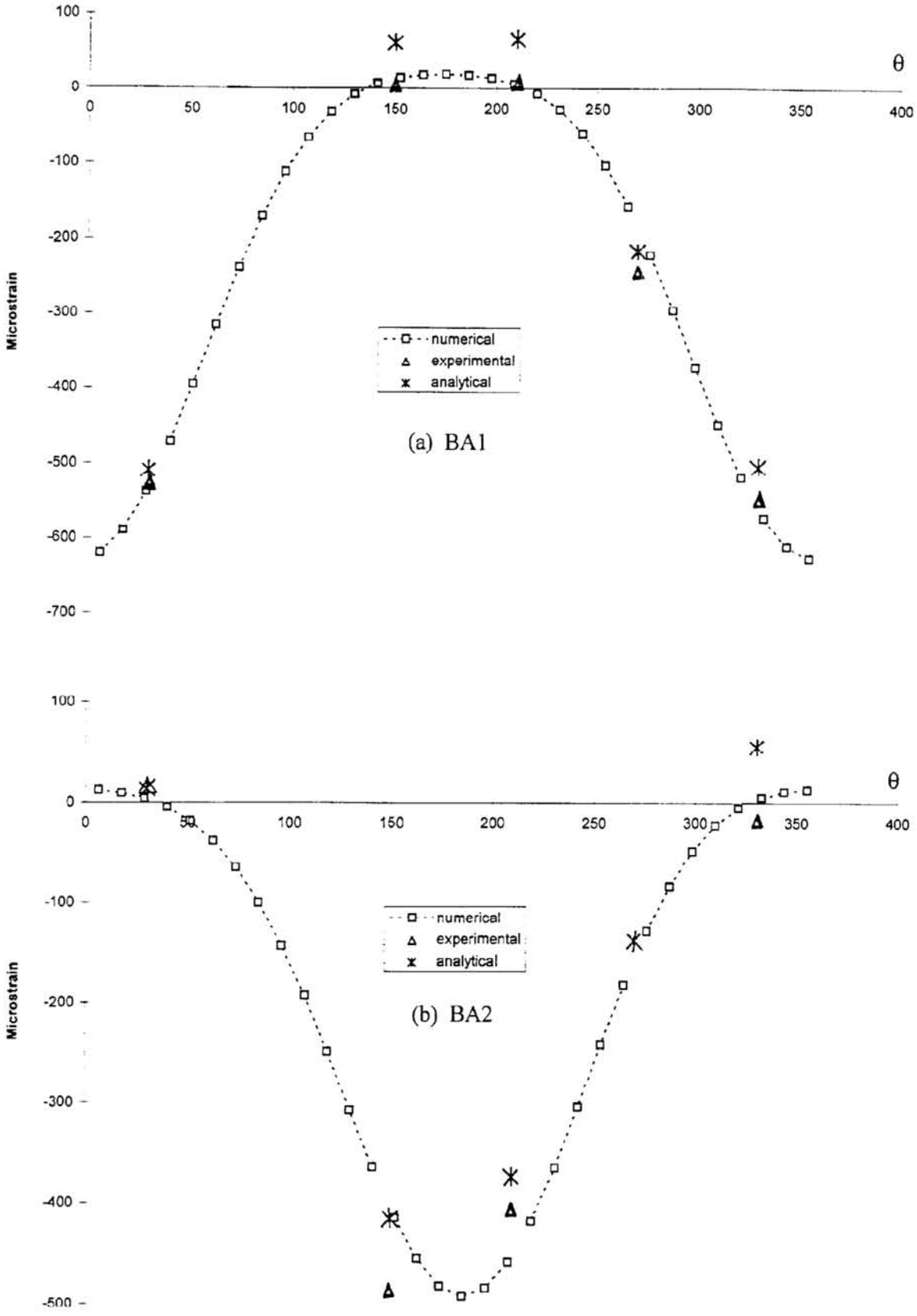


Figure 5.23 Comparison between numerical results, experimental data and analytical results